Clim Dyn (2012) 39:1457–1487
DOI 10.1007/s00382-011-1193-z

Mid-Holocene monsoons: a multi-model analysis of the inter-hemispheric differences in the responses to orbital forcing and ocean feedbacks

Y. Zhao · S. P. Harrison

Received: 19 May 2011 / Accepted: 7 September 2011 / Published online: 25 September 2011

Abstract The response of monsoon circulation in the northern and southern hemisphere to 6 ka orbital forcing has been examined in 17 atmospheric general circulation models and 11 coupled ocean–atmosphere general circulation models. The atmospheric response to increased summer insolation at 6 ka in the northern subtropics strengthens the northern-hemisphere summer monsoons and leads to increased monsoonal precipitation in western North America, northern Africa and China; ocean feedbacks amplify this response and lead to further increase in monsoon precipitation in these three regions. The atmospheric response to reduced summer insolation at 6 ka in the southern subtropics weakens the southern-hemisphere summer monsoons and leads to decreased monsoonal precipitation in northern South America, southern Africa and northern Australia; ocean feedbacks weaken this response so that the decrease in rainfall is smaller than might otherwise be expected. The role of the ocean in monsoonal circulation in other regions is more complex. There is no discernable impact of orbital forcing in the monsoon region of North America in the atmosphere-only simulations but a strong increase in precipitation in the ocean–atmosphere simulations. In contrast, there is a strong atmospheric response to orbital forcing over northern India but ocean feedback reduces the strength of the change in the monsoon although it still remains stronger than today. Although there are differences in magnitude and exact location of regional precipitation changes from model to model, the same basic mechanisms are involved in the oceanic modulation of the response to orbital forcing and this gives rise to a robust ensemble response for each of the monsoon systems. Comparison of simulated and reconstructed changes in regional climate suggest that the coupled ocean–atmosphere simulations produce more realistic changes in the northern-hemisphere monsoons than atmosphere-only simulations, though they underestimate the observed changes in precipitation in all regions. Evaluation of the southern-hemisphere monsoons is limited by lack of quantitative reconstructions, but suggest that model skill in simulating these monsoons is limited.

Keywords Monsoons · Orbital forcing · Ocean feedback · Palaeoclimate modelling intercomparison project · Coupled ocean–atmosphere simulations · Mid-Holocene climates · Palaeoclimate reconstructions

Y. Zhao (✉) · S. P. Harrison
School of Geographical Sciences, University of Bristol, Bristol BS4 1SS, UK
e-mail: yan.zhao@lsce.ipsl.fr

S. P. Harrison
e-mail: sandy.harrison@mq.edu.au

Y. Zhao
Laboratoire des Sciences du Climat et de l'Environment, CEA/CNRS/UVSQ, Saclay, France

S. P. Harrison
School of Biological Sciences, Macquarie University, North Ryde, NSW 2109, Australia

1 Introduction

Monsoons are defined as seasonally reversing wind systems in the tropics and subtropics, driven by thermal contrast between the land and the ocean which follows the seasonal cycle of insolation (Ramage 1971; Hastenrath 1994). Characteristically, wind flow is onshore during the summer and offshore in winter resulting in a seasonally contrasted precipitation regime with rainfall in summer and

dry conditions in winter. The Afro-Asian monsoon is the most pronounced example of this phenomenon and consists of three major components: the northern Africa monsoon (Hastenrath 1994), the Indian Monsoon (Lau et al. 2000) and the East Asian Monsoon (Tao and Chen 1987). However, monsoon-type climates are also characteristic of central and southwestern USA (Higgins et al. 1997), South America (Zhou and Lau 1998), southern Africa (e.g. Hastenrath 1994) and northern Australia (Davidson et al. 1983).

Palaeoenvironmental data show that there have been changes in regional precipitation patterns in monsoon regions on glacial-interglacial timescales. Pollen, plant and animal macrofossil, and lake-level evidence show dramatic changes in northern Africa, with conditions very much wetter than today across the present-day Sahara during the last interglacial (Petit-Maire 1989) and during the first half of the Holocene (Street-Perrott and Perrott 1993; Prentice et al. 2000). Pollen, lake-level and loess data from China indicate that the area affected by the East Asian monsoon was more prominent during the last interglacial (Huang et al. 2000; An 2000) and middle Holocene (Yu et al. 2000; An et al. 2000; Kohfeld and Harrison 2001; Shi et al. 1993; Wang et al. 2010). Changes were apparently more muted in northern India (Overpeck et al. 1996; Staubwasser and Weiss 2006) and in central and southwestern North America (Thompson and Anderson 2000; Harrison et al. 2003; Poore et al. 2005), but nevertheless palaeodata indicate increased monsoonal rainfall during the mid-Holocene in both regions. Palaeoenvironmental evidence from South America and Australia also document changes in the southern hemisphere monsoons on glacial-interglacial timescales. The South American monsoon was weaker than today during the mid-Holocene (Behling 1995; Haug et al. 2001; Cruz et al. 2005; Carré et al. in press). The Australian monsoon was stronger than present during the last glacial prior to ca 45 ka (Johnson et al. 1999; Miller et al. 1999), but there is more controversy about whether it was stronger or weaker in the mid-Holocene (see e.g. Wyrwoll and Miller 2001; Beaufort et al. 2010).

The observed changes in the monsoons over the last glacial-interglacial transition are a consequence of known changes in orbital forcing (Kutzbach and Otto-Bliesner 1982; Kutzbach and Guetter 1986). At the last glacial maximum (ca 21 ka), precessional parameters and thus the seasonal cycle of insolation, were similar to today. With the shift in the date of perihelion from mid-winter (at 21 ka and today) to mid-summer (in the early Holocene), the seasonal difference in insolation in the northern hemisphere was gradually enhanced to reach a maximum at ca 11 ka and gradually decreased thereafter. These changes in insolation are reflected in the waxing and waning of the northern-hemisphere monsoons. Similarly, broadscale changes in the southern hemisphere monsoons reflect that fact that the seasonal difference in insolation was minimal during the early to mid-Holocene and maximal at 21 ka and today. Although insolation changes are the primary cause of changes in the monsoons, modelling studies have shown that a variety of insolation-induced changes in land- and ocean-surface conditions modulate the response to the initial forcing. These feedbacks include e.g. changes in mid-latitude snow cover (Bush 2002), changes in vegetation cover (Kutzbach et al. 1996; Braconnot et al. 1999; Doherty et al. 2000) and changes in tropical sea-surface temperatures (Kutzbach and Liu 1997; Texier et al. 2000; Kutzbach et al. 2001). Given that monsoonal circulation is driven by the thermal contrast between the land and ocean, the role of changes in sea-surface temperatures is crucial and thus the role of ocean feedback on the global monsoons has been a major focus of modelling studies (e.g. Kutzbach and Liu 1997; Braconnot et al. 2000; Braconnot et al. 2004; Liu et al. 2004; Zhao et al. 2005; Ohgaito and Abe-Ouchi 2007).

Most investigations of the relative importance of direct insolation forcing and ocean feedback have focused on the mid-Holocene (6 ka), a time when the northern hemisphere ice sheets had all but disappeared but the northern-hemisphere seasonal difference in insolation was still high. Multiple studies have shown that the ocean amplifies orbitally-induced changes in the northern Africa monsoon, in part because differential ocean heating north and south of the equator strengthens onshore flow and in part because the lagged thermal response of the ocean relative to the land initiates monsoon onset earlier (Hewitt and Mitchell 1998). There are several studies of the role of ocean feedback on the Afro-Asian monsoon (Liu et al. 2004; Zhao et al. 2005; Ohgaito and Abe-Ouchi 2007; Marzin and Braconnot 2009; Wang et al. 2010). There have been far fewer studies of the role of ocean feedbacks on other northern hemisphere monsoons (although see Harrison et al. 2003; Liu et al. 2004), and only Liu et al. (2004) have attempted to evaluate the role of ocean feedback on both northern and southern hemisphere monsoons.

Liu et al. (2004) compared 6 ka simulations made with a low-resolution coupled ocean–atmosphere model, FOAM (Fast Ocean–Atmosphere Model: Jacob, 1997), and the atmosphere-only component of the same model. They confirmed earlier studies showing that ocean feedbacks amplify the insolation-induced enhancement of the northern Africa and North American monsoons. However, they suggested that ocean feedbacks damped the direct insolation-induced amplification of the Asian monsoon – a result which appears to be confirmed by later studies (e.g. Ohgaito and Abe-Ouchi 2007; Marzin and Braconnot 2009). Liu et al. (2004) showed that the atmospheric response to orbital forcing caused a reduction in the

southern hemisphere monsoons. However, the impact of ocean feedback differed regionally. Ocean feedback reinforced the insolation-induced reduction in monsoon precipitation over South America, minimised the reduction in rainfall over southern Africa, and reversed the orbitally-induced reduction in the northern Australia monsoon (see also Marshall and Lynch 2006). These differences in behaviour seem to be related to localised changes in ocean characteristics in the southern hemisphere. Ohgaito and Abe-Ouchi (2009) have shown that the effects of SST bias and the biases among the AGCMs on 6 ka precipitation enhancement over the Asian monsoon region were comparable. This opens up the possibility that the response may be sensitive to the treatment of the ocean circulation, and provides a motivation for the re-examination of the response of the global monsoons to orbital forcing and ocean feedback.

In this study, we capitalise on the existence of multiple simulations of the response to orbital forcing at 6 ka made in the Palaeoclimate Modelling Intercomparison Project. In its initial phase (PMIP1: Joussaume and Taylor 2000), PMIP focused on simulations with atmospheric general circulation models. In its subsequent phase (PMIP2: Harrison et al. 2002), the PMIP modelling groups have made simulations with fully-coupled ocean–atmosphere general circulation models. Analysis of the PMIP1 AGCM simulations allows us to diagnose the direct effects of orbital forcing on the northern and southern hemisphere monsoons. Comparison of the two sets of simulations allows us to examine the impacts of ocean feedback superimposed on the direct effects of orbital forcing. Although this does not strictly provide a diagnosis of the ocean feedback or isolation of synergistic effects (see e.g. Wohlfarht et al. 2004; Otto et al. 2009), we assume that the differences between the ensemble response of the atmosphere-only simulations and the ensemble response of the ocean–atmosphere simulations represents the broad-scale impact of ocean feedback on each monsoon system. We compare the simulated changes in precipitation in the two sets of experiments to a new quasi-global data set of pollen-based climate reconstructions (Bartlein et al. 2011) in order to evaluate how far the incorporation of ocean feedback produces a more realistic simulation of the mid-Holocene monsoons.

2 Analytical approach

The best way of separating the atmospheric response to orbital forcing and the oceanic feedback is to compare AGCM and OAGCM simulations made with the same model. This has been done for a few individual models (see e.g. Braconnot et al. 2000; Liu et al. 2004; Braconnot et al. 2004; Ohgaito and Abe-Ouchi 2007; Marzin and Braconnot 2009; Otto et al. 2009). Given that there is a considerable range in the response of different models to 6 ka forcing (see e.g. Joussaume et al. 1999; Zhao et al. 2005; Braconnot et al. 2007) it is important to check whether these results are representative of all the PMIP climate models. Unfortunately, the atmospheric component of each of the coupled models used in PMIP2 is different from the atmospheric-only version of that model used in PMIP1 and none of the PMIP2 modelling groups have made atmosphere-only simulations with the same version of the model. Since this precludes direct analysis of the ocean feedback for individual models, we have adopted a different strategy.

We first examine the suite of 11 ocean–atmosphere models archived in the PMIP database (http://www-lsce.cea.fr/pmip/) to determine whether the responses are similar from model to model, then we compare the ensemble response of these models with the ensemble response of the 17 atmosphere-only simulations archived in PMIP1 (http://www-lsce.cea.fr/pmip/). Comparison of the 0 ka (control) and 6 ka atmosphere-only experiments made with each model allows us to diagnose the direct response to orbital changes and derive an ensemble response for each of the monsoon systems. Comparison of the 0 ka (control) and 6 ka coupled simulations made with each model shows the combined response from orbital forcing and ocean feedback. Finally, on the assumption that differences between model versions are likely to be smaller than differences between models (an assumption broadly supported by comparison of the two models that contributed simulations with two versions in PMIP1 (LMD4/LMD5) and PMIP2 (MRI-fa/MRI-nfa), we have examined the ensemble of five models that ran atmosphere-only simulations in PMIP1 (CCM3/CCSM, ECHAM3/ECHAM5, LMD5/IPSL, MRI2/MRI-fa and UKMO/HadCM3: see Table 1) with an earlier version of the model they used in PMIP2 (hereafter referred to as the 5-member ensemble), as a check on the robustness of the conclusions drawn from the larger ensemble.

2.1 Orbital forcing

The major factor influencing the 6 ka climate is the change in orbital forcing; the change in forcing was specified from Berger (1978) and is identical in the two sets of experiments (Table 1). At 6 ka, insolation was increased (compared to today) during the boreal summer/austral winter half-year and decreased (compared to today) during the boreal winter/austral summer half-year (Fig. 1). The overall impact of these changes varies with latitude: the mean annual forcing was positive in the extratropics and slightly negative (up to 13 W/m^2) in the tropical zone of both hemispheres (Fig. 1b). The timing of the changes is

Table 1 Details of the models used in these analyses

Model code	PMIP name	Model designation	Reference
AGCM models from PMIP1			
BMRC	BMRC	Bureau of Meterological Research Centre (Australia)	Colman and McAvaney (1995)
CCC2	CCC2	Canadian Centre for Climate Modelling and Analysis (Canada)	Vettoretti et al. (1998)
CCM3	CCM3	NCAR Climate Community Model (USA) run at CCR	Kiehl et al. (1996)
CCSR1	CCSR1	Centre of Climate System Research (Japan)	Numaguti et al. (1997)
CNRM2	CNRM2	Center National de Recherches Météorologiques (France)	Deque et al. (1994)
CSIRO	CSIRO	Commonwealth Scientific and Industrial Research Organisation (Australia)	Gordon and O'Farrell (1997)
ECHAM3	ECHAM3	Max-Planck Institut für Meterologie (Germany) run at Bremen Univ.	Lorenz et al. (1996)
GEN2	GEN2	National Center for Atmopheric Research (USA) GENESIS model	Pollard et al. (1998)
GFDL	GFDL	Geophysical Fluid Dynamics Laboratory (USA)	Gordon and Stern (1982)
GISS	GISS-IIP	Goddard Institute for Space Studies (USA)	Hansen et al. (1997)
LMD4	LMD4	Laboratoire de Météorologie Dynamique (France) at LSCE	Masson and Joussaume (1997)
LMD5	LMD5	Laboratoire de Météorologie Dynamique (France) at LSCE	Masson and Joussaume (1997)
MRI2	MRI2	Meteorological Research Institute (Japan)	Kitoh et al. (1995)
UGAMP	UGAMP	UK Universities Global Atmospheric Modelling Programme	Hall and Valdes (1997)
UIUC11	UIUC11	University of Illinois Urbana-Champaign (USA)	Schlesinger et al. (1997)
UKMO	UKMO	UK Meteorological Office Unified Model	Hewitt and Mitchell (1997)
YONU	YONU	Yonseï University (Korea)	Tokioka et al. (1984)
OAGCM models from PMIP 2			
CCSM	CCSM3	Community Climate System Model run at the Natioanl Center for Atmospheric Research, Boulder, Colorado (USA)	Otto-Bliesner et al. (2006)
ECBILT	ECBILTCLIO	Institut d'Astronomie et de Geophysique Georges Lemaitre, Louvain-la-Neuve (Belgium)	Vries and Weber (2005)
ECHAM5	ECHAM5-MPIOM1	Max-Planck Institut für Meterologie (German) run at University of Kiel	Roeckner et al. (2003); Marsland et al. (2003); Haak et al. (2003).
FGOALS	FGOALS-v1.g	Institute of Atmospheric Physics (China)	Yu et al. (2002); Yu et al. (2004)
FOAM	FOAM	Fast Ocean Atmosphere Model run at Bristol University	Jacob et al. (2001)
GISS	GISSmodelE	Goddard Institute for Space Studies (USA)	Schmidt et al. (2005)
HadCM3	UBRIS-HadCM3M2	UK Meterological Unified Model run at Bristol University (UK)	Gordon et. al. (2000)
IPSL	IPSL-CM4-V1-MR	L'Institut Pierre-Simon Laplace model run at LSCE (France)	Marti et al. (2005)
MIROC	MIROC3.2	CCSR, NIES and FRCGC (Japan)	K-1 Model Developers (2004)
MRI-fa	MRI-CGCM2.3fa	Meterological Research Institute (Japan) coupled GCM with flux adjustments	Yukimoto et al. (2006)
MRI-nfa	MRI-CGCM2.3nfa	As above without flux adjustments	Yukimoto et al. (2006)

also not symmetric: the maximum increase in insolation (ca 25 W/m^2) occurred in July in the northern extratropics and northern tropics, August in the northern equatorial zone and September in the southern equatorial zone and southern tropics, and October in the southern extratropics (Fig. 1c). Thus, while the major increase in insolation is focused on the summer in the northern hemisphere, there is a delay in the southern hemisphere so that austral spring rather than mid-winter is characterised by increased insolation.

2.2 PMIP1 AGCM experiments

Seventeen models were used to examine the atmospheric response to orbital forcing at 6 ka during the first phase of PMIP (Table 1). Two simulations were made with each model: a 0 ka (control) and a 6 ka experiment. Orbital parameters at 0 and 6 ka were specified from Berger (1978). Ocean- and land-surface conditions were specified to be the same in the 6 and 0 ka experiments. Atmospheric CO_2 concentration was lower than either modern or pre-

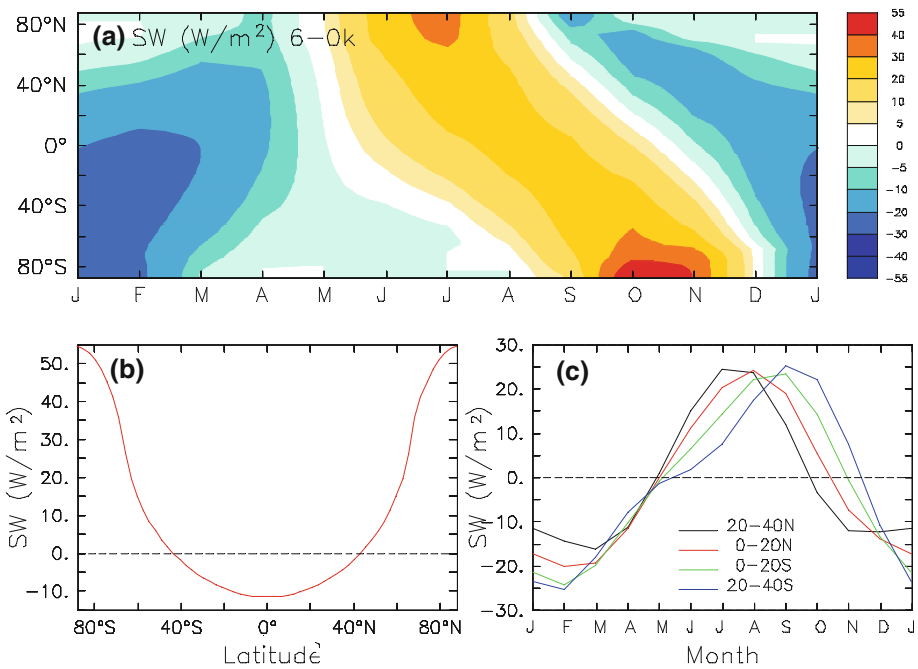

Fig. 1 Changes in orbital forcing at 6 ka: **a** the difference in the seasonal cycle of incoming radiation (insolation) at the top of the atmosphere (W/m^2) between the mid-Holocene (6 ka) and today; **b** the change in mean annual forcing (W/m^2) by latitude; **c** the change in the seasonal cycle of forcing averaged for the northern tropics (20–40°N), the northern equatorial zone (0–20°N), the southern equatorial zone (0–20S) and the southern tropics (20–40°S)

industrial levels at 6 ka (Monnin et al. 2004). Most modelling groups used a modern level of 345 ppm in the control experiments and 280 ppm at 6 ka; modelling groups that made use of a pre-existing control simulation with a CO_2 concentration different from the recommended level reduced the CO_2 concentration by a comparable ratio (i.e. 345/280*control) in the 6 ka experiments. The simulations were run for different lengths of time but the archived results for each model are a 1-year average from the final years of the simulation.

2.3 PMIP2 OAGCM experiments

Eleven coupled ocean–atmosphere models were used to examine the combined response to orbital forcing at 6 ka in PMIP2 (Table 2). Two simulations were made with each model: a 0 ka (control) and a 6 ka experiment. Orbital parameters at 0 ka and 6 ka were specified from Berger (1978). Land-surface parameters and greenhouse gas concentrations were prescribed to be identical in the two experiments. Pre-industrial CO_2 concentrations of 280 ppm were used in both the control and 6 ka experiments. Each of the coupled-model simulations was run for several hundred years, sufficient for surface climate fields to reach quasi-equilibrium, and the archived results are a 100-year average of the final years of the simulation.

The treatment of CO_2 concentration differs between the PMIP1 AGCM and PMIP2 OAGCM sets of experiments. The change in CO_2 concentration of 65 ppm is equivalent to an annual radiative forcing of 1.12 W/m^2, which is considerably smaller than the ca 5-20 W/m^2 increase in seasonal radiative forcing in the monsoon zone (40°S to 40°N: see Fig. 1) caused by the change in orbital forcing. Decreasing CO_2 concentration by 65 ppm produced a cooling of 0.1 K in global annual mean land surface temperature in experiments made with the HadCM2 model (Hewitt and Mitchell 1996), and a global cooling of 0.5 K in ECHAM3/LSG (Voss and Mikolajewicz 2001). Voss and Mikolajewicz (2001) pointed out that the warming due to insolation changes exceeds the CO_2-induced cooling in the Northern Hemisphere. Furthermore, the CO_2-induced response of precipitation is very weak and not significant. Thus, this difference in experimental design is unlikely to be responsible for major differences between the two sets of experiments in terms of monsoon precipitation.

Table 2 Boundary conditions used for control and 6 ka experiments in PMIP1 and PMIP 2

	Control simulation	6 ka BP
Orbital parameters		
Eccentricity	0.01672	0.018682
Axial title (°)	23.446	24.105
Perihelion-180 (°)	102.04	0.87
CO_2 concentration		
PMIP1	345 ppm or C_{ctrl}	280 ppm or C_{ctrl}*(280/345)
PMIP2	280 ppm	280 ppm

2.4 Analyses

We present analyses of the six major monsoon regions: northern Africa, Asia, North America, southern Africa, northern Australia and South America (Table 3). We characterise the response of the monsoons by analysing changes in surface climate fields (mean monthly temperature, precipitation), atmospheric circulation at the surface and aloft (mean monthly sea level pressure, surface winds, winds at pressure levels), and measures of the vertical motion (vertical velocity: omega) and moisture (water vapour) content of the atmospheric column. Upper-level winds, omega and water vapour content are not available from the PMIP1 AGCM experiments. We express mean changes in climate variables on a regional basis using definitions of each monsoon region (Table 3) proposed by Liu et al. (2004), except in the Asian sector where we treat the Indian, East Asian and and Southeast Asian Indian monsoon systems separately. Studies of the monsoon under modern climate conditions show that each of these subsystems has a distinctive spatio-temporal structure as well as different energetics (Lau et al. 2000; Chang 2004), and thus should be examined separately.

We use the standard deviation (SD) around the ensemble mean results for each region to gauge the significance of simulated changes between the control and 6 ka PMIP1 AGCM and PMIP2 OAGCM experiments. It is not possible to estimate whether the change between the control and 6 ka experiments is significantly greater than interannual variability in specific regions for the PMIP1 AGCM simulations because only climatological means for each model are archived in the PMIP database. However, the significance of the simulated change between the control and 6 ka simulations for each PMIP2 OAGCM model has been calculated using a Student *t* test, and results that are significant at the 95% level are indicated in Fig. 5.

Table 3 Definition of the spatial domain of each of the monsoon systems, used for calculating e.g. mean climate changes

Monsoon region	Spatial domain
Northern Africa	12–30°N, 20°W–30°E
Asian monsoon	
India	20–40°N, 70–100°E
East Asia	20–50°N, 100–150°E
Southeast Asia	7.5–30°N, 105–127.5°E
North America	20–40°N, 95–120°W and 0–20°N, 60–120°W
Southern Africa	5–25°S, 0–50°E
Northern Australia	5–25°S, 110–150°E
South America	5–25°S, 30–70°W

We compare the simulated changes in regional climates with a new gridded data set of quantitative climate reconstructions produced by Bartlein et al. (2011). This data set provides reconstructions of six variables (the accumulated temperature sum during the growing season, growing degree days, GDD5; mean temperature of the warmest month, MTWA; mean temperature of the coldest month, MTCO; mean annual temperature, MAT; mean annual precipitation, MAP; and plant-available moisture, alpha) for the Last Glacial Maximum and for 6 ka—although not all variables are available for every region. The data were produced by combining existing site-based reconstructions derived using various statistical techniques and/or model inversion. In addition to providing a robust measure of the mean climate change, this data set also provides estimates of the uncertainty of the reconstructions based on comparison between the results obtained at each site using different reconstruction methods. The reconstructed anomalies for each climate variable are given for a regular $2 \times 2^{\circ}$ grid, where the value of the anomaly was obtained by simple averaging, and the uncertainty as a pooled estimate of the standard error.

Although a comprehensive synthesis of available quantitative climate reconstructions, the Bartlein et al. (2011) set does not contain information for the South America and northern Australia monsoon regions. In our comparisons of simulated and reconstructed climate, we therefore focus on the northern Africa, India, East Asia, North America and southern Africa monsoons. We extracted the reconstructed changes in climate for each of the monsoon regions, as defined in Table 3. There are too few reconstructions (only 2–4 grids with significant anomalies) within the southern Africa monsoon domain and for the purposes of model evaluation we enlarged the domain by expanding the latitudinal range from 5–25° S to 5–35°S. Simulated climate variables were bi-linearly interpolated to the same $2 \times 2^{\circ}$ grid for ease of comparison. This changes the values of the regional mean slightly compared with those obtained directly from averaging at the models grid-cell resolution, but does not affect the overall signal.

The Bartlein et al. (2011) data set does not provide reconstructions of summer precipitation, but the contribution of winter rainfall to the annual in most monsoon areas is comparatively small and thus the comparison of simulated and reconstructed MAP provides a good test of model performance. We have also compared simulated and reconstructed summer (MTWA) and year-round temperature (MAT) over land for each monsoon region. To derive estimates of the mean changes in MAP, MAT and MTWA for each monsoon region, for comparison with the model-ensemble regional means, we have weighted the individual reconstructions (by 1 for those points that are significant, i.e. those that exceed twice the pooled standard error of the

reconstructions, and by 0.5 for those points that are non-significant but nevertheless show changes coherent with the regional signal). Given that the data are not uniformly distributed across each region, we have checked to see that they are representative of the monsoon region as a whole by examining the difference between the simulated climate across the domain as a whole and for those grid cells for which there are reconstructions.

3 The atmospheric response to orbital forcing: analysis of the PMIP1 AGCM experiments

Examination of the simulations made with individual models shows that the climate responses to orbital forcing, and the mechanisms which give rise to these responses, are the same in all of the models. Thus, here we discuss the control and 6 ka experiments in terms of the behaviour of the ensemble of models, noting that the large-scale patterns are the same in the 5-member ensemble (i.e. the ensemble of those models that ran atmosphere-only simulations in PMIP1 with an earlier version of the atmospheric model they used in PMIP2) as in the 11-member OAGCM ensemble.

As might be expected, the seasonal evolution of the monsoons in the PMIP1 AGCM control simulations mirrors the latitudinal shift in the timing of maximum insolation. The high temperatures (>30°C) experienced in the northern subtropics during boreal summer (Fig. 2a) results in a northward displacement of the inter-tropical convergence zone (ITCZ) and of the subtropical anticyclones over the Atlantic and Pacific Oceans (Fig. 2b). The mean position of the ITCZ is more northerly (ca 15–20°N) over the continents than over the adjacent oceans (ca 10°N) because of the differential warming of land and sea. As a result of the deep thermal lows developed over the continents, the northern subtropical land masses are characterised by strong onshore flow (Fig. 2b) allowing moisture-bearing winds to penetrate far inland. As a result (Fig. 2c), northern Africa, northern India, eastern China, central America and the southwestern United States are characterised by heavy monsoon precipitation (>6 mm/per day during boreal summer: June, July, August). During boreal autumn and winter (i.e. September through March), maximum insolation occurs

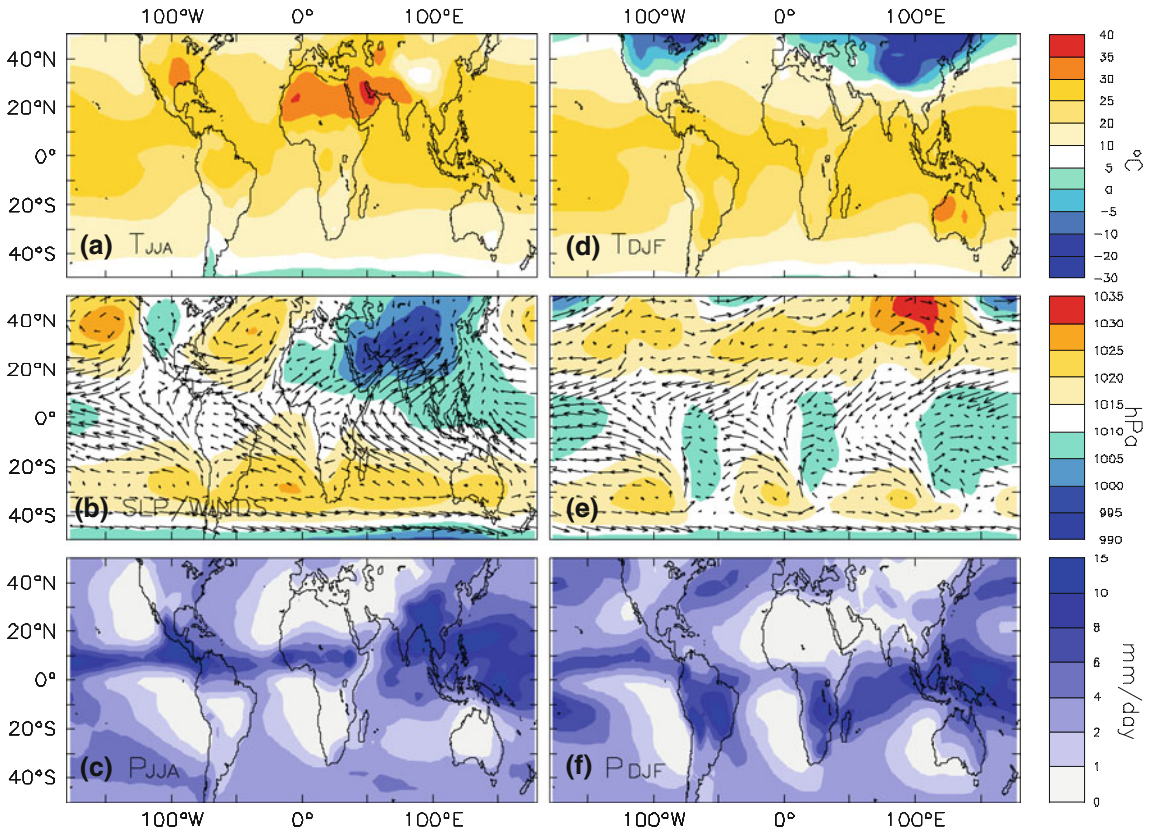

Fig. 2 Simulated modern climate, based on the 17-model ensemble mean of the AGCM control simulations: **a** surface temperature (°C) during boreal summer/austral winter (June, July, August: JJA), **b** sea level pressure (hPa) and surface wind patterns during boreal summer/austral winter (JJA), **c** precipitation (mm/day) in boreal summer/austral winter (JJA), **d** surface temperature (°C) during boreal winter/austral summer (December, January, February, DJF), **e** sea level pressure (hPa) and surface wind patterns during boreal winter/austral summer (DJF), **f** precipitation (mm/day) in boreal winter/austral summer (DJF)

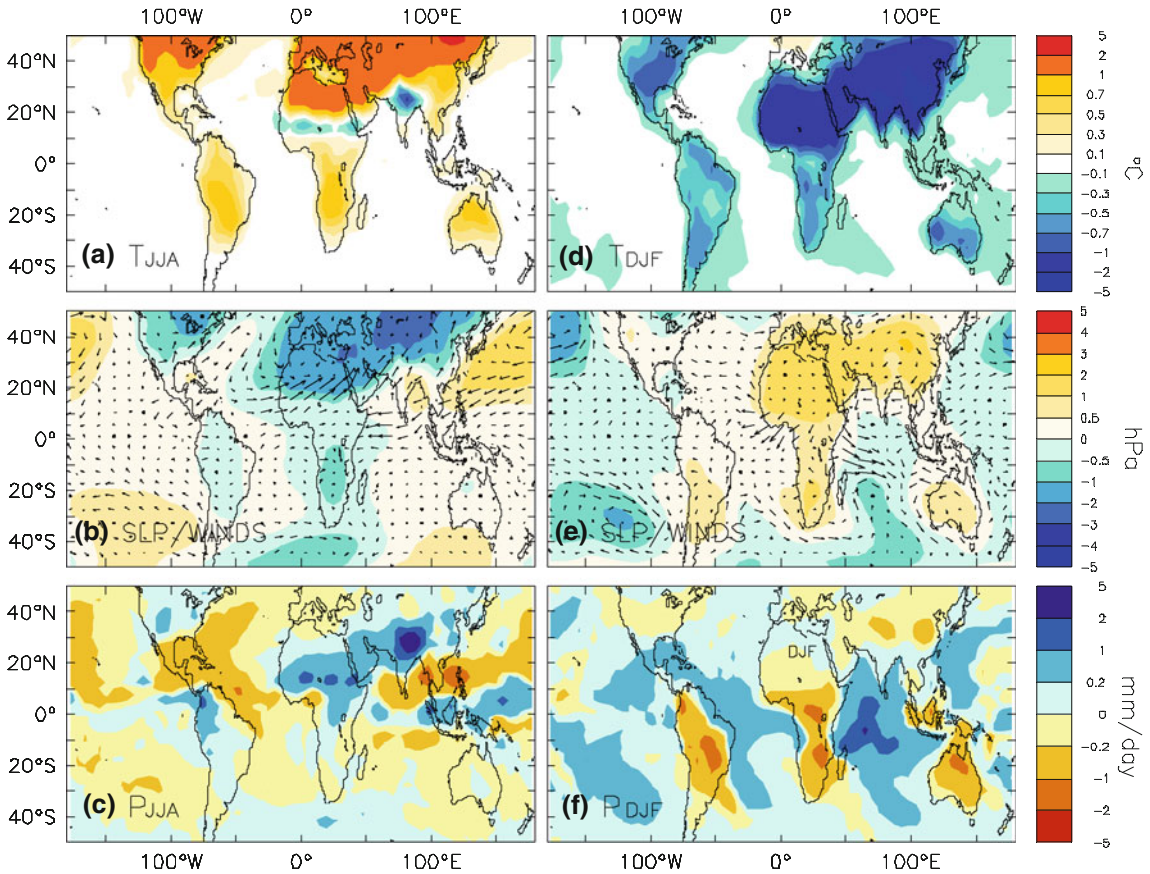

Fig. 3 Changes in climate between 6 ka and present day, based on the difference between the 17-model ensemble mean of the AGCM control and 6 ka climate simulations: **a** surface temperature (°C) during boreal summer/austral winter (June, July, August: JJA), **b** sea level pressure (hPa) and surface wind patterns during boreal summer/austral winter (JJA), **c** precipitation (mm/day) in boreal summer/austral winter (JJA), **d** surface temperature (°C) during boreal winter/austral summer (December, January, February, DJF), **e** sea level pressure (hPa) and surface wind patterns during boreal winter/austral summer (DJF), **f** precipitation (mm/day) in boreal winter/austral summer (DJF)

in the southern hemisphere and thus the ITCZ is displaced southward towards the equator (Fig. 2e). The cooling of the northern extratropics results in the development of strong anticyclones over the land. As a result, surface flow from the northern continents is offshore and dry conditions prevail in the northern monsoon regions. The oceanic nature of the southern hemisphere means that the warming in the southern subtropics during austral summer (Fig. 2d) is not as pronounced as the warming over the northern subtropics during boreal summer. Nevertheless, low pressure systems develop over the southern continents (Fig. 2e) and the resultant enhancement of onshore flow results in monsoonal precipitation (>6 mm/per day during austral summer: December, January, February) over southern Brazil, southern Africa and northern Australia (Fig. 2f).

The change in orbital forcing at 6 ka results in an increase in northern hemisphere insolation during boreal summer. This results in higher temperatures (>1°C) over the northern land masses (Fig. 3a). As a consequence of the change in temperature gradient the simulated position of the ITCZ is further north (Fig. 3b), and the subtropical anticyclones are also stronger and located in a more northerly position, than in the control simulations. The thermal low over the northern continents was deeper (>2 hPa), leading to a strengthening of onshore flow. As a result, monsoon rainfall penetrated further inland and the total amount of rainfall during the monsoon season was increased over northern Africa, India, China and the southwestern USA (Fig. 3c). The substantial strengthening of the Afro-Asian monsoon resulted in increased cloudiness and evaporation, and hence lower temperatures, along the monsoon front in northern Africa and India. Reduced insolation in the northern subtropics during boreal winter resulted in the strengthening of the anticyclones over the northern continents (Fig. 3e) and a concomitant increase in the strength of the winter monsoons. The northern continents are drier in winter than in the control simulations (Fig. 3g). However, insolation is also reduced in the southern subtropics during boreal winter/austral summer and temperatures over the southern continents are lower

than in the control simulations (Fig. 3d). This minimises the southward shift of the ITCZ during boreal winter/austral summer. The low-pressure systems seen over the southern continents in the control simulations in austral summer are not as apparent at 6 ka (Fig. 3e), and the development of the southern hemisphere monsoons is therefore suppressed.

4 The role of direct orbital forcing and ocean feedback on individual monsoon systems

We investigate the contribution of change in orbital forcing and ocean feedback on the response of individual monsoons. For comparison with previous studies, we express mean changes in climate variables on a regional basis using the same definitions of each monsoon region (Table 3) as Liu et al. (2004), except in the Asian sector where we treat the Indian, East Asian and Southeast Asian monsoon systems separately.

4.1 Northern Africa

The response of the northern Africa monsoon to mid-Holocene orbital forcing has been the subject of numerous studies (e.g. Kutzbach and Liu 1997; Hewitt and Mitchell 1998; Braconnot et al. 1999; Joussaume et al. 1999; Otto-Bliesner 1999; Braconnot et al. 2002; Kutzbach et al. 2001; Zhao et al. 2005); our analyses essentially confirm previous studies in both the patterns of climate change and the underlying mechanisms. The direct effect of the orbitally-induced change in summer insolation leads to warming compared to present over northern Africa by ca 0.55°C (Fig. 3a, Table 4); as a result, land-sea contrast is enhanced resulting in increased low-level convergence into the monsoon low over northern Africa. Onshore winds are stronger and the monsoon front is more northerly than in the control simulations (Fig. 3b), and precipitation over northern Africa is increased by ca 0.39 mm/day (Fig. 3c, Table 5) and by 0.38 mm/day in the 5-member ensemble. Oceanic feedback, associated with a strengthening of the Atlantic dipole structure with warmer sea-surface temperatures (SSTs) to the north of 5–10°N and colder SSTs to the south (Fig. 4a), produces a somewhat stronger low-level convergence than does orbital forcing alone (Fig. 4b), a more northerly migration of the monsoon front, and thus a further enhancement of monsoon precipitation (ca 0.73 mm/day for the 11-member and ca 0.68 mm/day for the 5-member ensemble) over northern Africa (Fig. 4c, Table 5). The difference in the magnitude of monsoon enhancement between the two sets of experiments is significant at the 99% level (Table 6). The Atlantic dipole structure is created by a combination of increased insolation and a strong wind-evaporation feedback around 15°N that leads to additional surface warming (Kutzbach and Liu 1997; Zhao et al. 2005). The system is also sustained by a southward Ekman drift, which delays the SST increase around 5°N and thus sharpens the dipole (Zhao et al. 2005). Previous studies have suggested that ocean feedback, and specifically the persistence of cool SSTs in spring when the land-surface is beginning to warm, produces an early onset of the northern African monsoon (Hewitt and Mitchell 1998). This tendency is apparent but not pronounced in the PMIP2 OAGCM simulations (not shown).

4.2 Asia

The Asian summer monsoon consists of two main components: the Indian monsoon and East Asian monsoon; the latter is sometimes subdivided into an East Asian and Southeast Asian domain. Although these monsoon systems are linked, they differ in dynamical structure (Lau et al. 2000; Chang 2004). There have been only a few analyses of the Asian monsoons during the mid-Holocene (though see Ohgaito and Abe-Ouchi 2007; Marzin and Braconnot 2009; Wang et al. 2010).

The Indian monsoon system (Fig. 2b) is dominated by convection in the Indian monsoon trough. This is part of a clockwise gyre over the Indian Ocean, which links southeasterly winds associated with the Mascarene High in the southern hemisphere (centred at ca 30°S) via the northerly and northwesterly flow of the Somali Jet, and thence into the Indian monsoon trough (Krishnamurti and Bhalme 1976). The moisture-laden winds divide on reaching the southernmost point of the Indian Peninsula into the Arabian Sea Branch and the Bay of Bengal Branch. The Arabian Sea Branch brings precipitation to coastal areas, west of the Western Ghats. The Bay of Bengal Branch flows towards northeastern India, picking up additional moisture from the Bay of Bengal and bringing precipitation to the Eastern Himalayas and the Indo-Gangetic Plain. Moisture transport is essential for the formation and maintenance of monsoon precipitation (Webster et al. 1998). The main source of moisture is evaporation from the South Indian Ocean and the Arabian Sea (Sadhuram and Kumar 1988; Ninomiya and Kobayashi 1999; Lim et al. 2002). The establishment of the monsoon circulation and precipitation is determined by the annual cycle of SSTs in the Indian Ocean; interannual variations in the strength of the monsoon are linked to variations in SSTs, particularly in the Arabian Sea (Shukla 1975; Rao and Goswami 1988; Clark et al. 2000). Thus, a cooler-than-normal Arabian Sea leads to reduced Indian rainfall and vice versa. However, the strength of the Indian summer monsoon is also related to the strength of the Mascarene High and the Somali Jet

Table 4 Change in simulated annual mean (ann) and summer (summ: June, July, August: JJA in northern hemisphere and December, January, February: DJF in southern hemisphere) temperature for each model for each of the monsoon domains (Unit: °C)

Model			Northern Africa		Indian		East Asian		Southeast Asian	
Type	No	Code	ann	summ	ann	summ	ann	summ	ann	summ
AGCM	1	BMRC	−0.91	−0.07	−1.01	0.28	−0.08	−0.93	−0.08	−0.93
AGCM	2	CCC2	−0.70	0.66	−1.19	0.18	0.10	−0.52	0.10	−0.52
AGCM	3	CCM3	−0.60	0.97	−0.56	0.60	−0.07	−0.39	−0.07	−0.39
AGCM	4	CCSR1	−0.23	0.92	−0.94	0.42	0.41	−0.50	0.41	−0.50
AGCM	5	CNRM2	−0.43	0.51	−0.64	0.32	0.16	−0.30	0.16	−0.30
AGCM	6	CSIRO	−0.20	0.98	−0.61	1.01	0.13	−0.24	0.13	−0.24
AGCM	7	ECHAM3	−0.74	0.80	−0.53	0.09	0.11	−0.52	0.11	−0.52
AGCM	8	GEN2	−0.51	0.27	−0.95	0.16	0.12	−0.39	0.12	−0.39
AGCM	9	GFDL	−0.38	0.54	−0.94	0.22	0.20	−0.60	0.20	−0.60
AGCM	10	GISS	−0.94	0.21	−1.28	−0.25	−0.19	−0.56	−0.19	−0.56
AGCM	11	LMD4	−0.45	0.32	−1.26	0.25	−0.10	−0.63	−0.10	−0.63
AGCM	12	LMD5	−0.56	0.28	−0.50	0.31	0.19	−0.37	0.19	−0.37
AGCM	13	MRI2	−0.68	0.09	−1.20	−0.23	−0.11	−0.34	−0.11	−0.34
AGCM	14	UGAMP	−0.09	0.90	−0.68	0.54	0.06	−0.48	0.06	−0.48
AGCM	15	UIUC11	−0.46	0.51	−1.69	−0.27	0.09	−0.59	0.09	−0.59
AGCM	16	UKMO	−0.25	0.53	−0.69	0.49	0.14	−0.31	0.14	−0.31
AGCM	17	YONU	−0.40	0.87	−0.63	0.80	0.13	−0.50	0.13	−0.50
		Mean	−0.50	0.55	−0.90	0.29	−0.48	0.08	−0.48	0.08
		SD	0.24	0.33	0.34	0.35	0.20	0.15	0.16	0.15
OAGCM	1	CCSM	−0.57	−0.04	−0.63	0.54	−0.21	−0.52	−0.21	−0.52
OAGCM	2	ECBILT	−0.26	0.17	−0.26	0.30	−0.06	−0.21	−0.06	−0.21
OAGCM	3	ECHAM5	−1.13	−0.41	−0.88	−0.03	0.05	−0.13	0.05	−0.13
OAGCM	4	FGOALS	−0.93	−0.87	−0.55	0.33	0.01	−0.28	0.01	−0.28
OAGCM	5	FOAM	−0.60	0.40	−0.30	0.73	−0.06	−0.52	−0.06	−0.52
OAGCM	6	GISS	−1.87	−1.48	−1.09	−0.49	−0.48	−0.92	−0.48	−0.92
OAGCM	7	HadCM3	−0.75	−0.06	−0.61	0.23	0.05	−0.59	0.05	−0.59
OAGCM	8	IPSL	−1.18	−0.47	−1.39	−0.44	−1.21	−1.51	−1.21	−1.51
OAGCM	9	MIROC	−1.13	−0.33	−1.06	−0.12	−0.14	−0.75	−0.14	−0.75
OAGCM	10	MRI-fa	−0.44	0.25	−0.78	−0.06	−0.19	−0.43	−0.19	−0.43
OAGCM	11	MRI-nfa	−0.61	0.05	−0.80	−0.18	−0.24	−0.46	−0.24	−0.46
		Mean	−0.86	−0.25	−0.76	0.07	−0.45	−0.23	−0.58	−0.23
		SD	0.45	0.55	0.34	0.39	0.35	0.36	0.38	0.36

Model			North America		Southern Africa		Northern Australia		South America	
Type	No	Code	ann	summ	ann	summ	ann	summ	ann	summ
AGCM	1	BMRC	−0.05	1.09	−0.08	−0.93	−0.19	−1.23	0.04	−0.51
AGCM	2	CCC2	−0.20	0.39	0.10	−0.52	0.27	−0.24	0.03	−0.45
AGCM	3	CCM3	0.03	0.76	−0.07	−0.39	0.08	−0.12	−0.03	−0.64
AGCM	4	CCSR1	−0.16	0.76	0.41	−0.50	0.01	−0.23	0.26	−0.17
AGCM	5	CNRM2	−0.20	0.68	0.16	−0.30	0.12	−0.74	0.30	−0.35
AGCM	6	CSIRO	−0.18	0.50	0.13	−0.24	0.35	−0.32	0.06	−0.44
AGCM	7	ECHAM3	−0.22	0.31	0.11	−0.52	0.38	−0.30	0.28	0.00
AGCM	8	GEN2	−0.14	0.51	0.12	−0.39	0.21	−0.36	0.08	−0.37
AGCM	9	GFDL	0.03	1.08	0.20	−0.60	0.12	−0.27	−0.08	−0.68
AGCM	10	GISS	−0.58	−0.13	−0.19	−0.56	−0.06	−0.53	−0.18	−0.67
AGCM	11	LMD4	−0.14	0.38	−0.10	−0.63	−0.01	−0.76	−0.05	−0.49

Table 4 continued

Model			North America		Southern Africa		Northern Australia		South America	
Type	No	Code	ann	summ	ann	summ	ann	summ	ann	summ
AGCM	12	LMD5	−0.18	0.80	0.19	−0.37	0.28	−0.05	0.09	−0.42
AGCM	13	MRI2	−0.08	0.43	−0.11	−0.34	0.32	0.17	−0.08	−0.36
AGCM	14	UGAMP	−0.25	0.50	0.06	−0.48	0.22	0.05	0.06	−0.28
AGCM	15	UIUC11	−0.33	0.25	0.09	−0.59	0.15	−0.05	−0.19	−0.41
AGCM	16	UKMO	−0.02	0.72	0.14	−0.31	0.17	−0.18	0.14	−0.33
AGCM	17	YONU	−0.25	0.39	0.13	−0.50	0.07	0.07	0.01	−0.33
		Mean	−0.48	0.55	0.08	−0.48	0.15	−0.30	0.04	−0.41
		SD	0.16	0.30	0.15	0.16	0.15	0.35	0.14	0.17
OAGCM	1	CCSM	−0.26	0.45	−0.21	−0.52	−0.03	−0.40	−0.17	−0.51
OAGCM	2	ECBILT	−0.16	0.09	−0.06	−0.21	0.06	−0.24	−0.07	−0.22
OAGCM	3	ECHAM5	−0.16	0.29	0.05	−0.13	0.23	−0.07	0.06	−0.10
OAGCM	4	FGOALS	−0.12	0.64	0.01	−0.28	0.04	0.05	−0.04	−0.36
OAGCM	5	FOAM	0.03	0.70	−0.06	−0.52	0.32	−0.26	0.11	−0.36
OAGCM	6	GISS	−0.46	0.28	−0.48	−0.92	−0.18	−0.49	−0.52	−0.86
OAGCM	7	HadCM3	0.04	1.21	0.05	−0.59	−0.23	−0.29	0.22	−0.44
OAGCM	8	IPSL	−1.25	−0.70	−1.21	−1.51	−1.23	−1.75	−1.19	−1.70
OAGCM	9	MIROC	−0.23	0.59	−0.14	−0.75	−0.26	−0.62	−0.21	−0.45
OAGCM	10	MRI-fa	−0.26	0.36	−0.19	−0.43	0.04	−0.35	−0.19	−0.34
OAGCM	11	MRI-nfa	−0.56	0.12	−0.24	−0.46	−0.16	−0.58	−0.27	−0.51
		Mean	−0.58	0.37	−0.23	−0.58	−0.13	−0.45	−0.21	−0.53
		SD	0.38	0.47	0.36	0.38	0.41	0.48	0.38	0.43

(Krishnamurti and Bhalme 1976; Xue et al. 2003). When the Mascarene High is anomalously strong, moisture transport from the Southern Hemisphere by the Somali Jet via the Arabian Sea and into the Indian subcontinent is enhanced, resulting in increased precipitation.

The summer monsoon over East Asia (Fig. 2b) is dominated by convection in the Western North Pacific monsoon trough, which occurs at the confluence between the southwesterly monsoon and southeast trade winds in the North Pacific. The Western North Pacific High and East Asian subtropical front are located to the north of the Western North Pacific monsoon trough. The Western North Pacific High is crucial in determining the intensity and location of the monsoon rain belt (Tao and Chen 1987). As the Western North Pacific High moves northward, the monsoon rainfall belt also shifts northward. The movement of Western North Pacific High is strongly affected by convection in the Western North Pacific monsoon trough (Wang et al. 2001). Again, moisture transport is essential for the formation and maintenance of monsoon precipitation. The East Asian monsoon region is influenced by moisture sources from both the Indian Ocean and the west Pacific Ocean (Li et al. 2008). The South China Sea (4°–20°N) supplies moisture for the East Asian monsoon where three low level jets converge: southwesterly flow from the northern Indian Ocean; southerly flow from the cross-equatorial jet and southeasterly flow from the southeast flank of Western North Pacific High (Fig. 2b). SSTs in the South China Sea influence the timing and intensity of the South China Sea monsoon, which is a part of East Asian monsoon (Ding 1994). Anomalously warm SSTs in the South China Sea lead to early onset of the South China Sea monsoon; a strong South China Sea monsoon usually leads to more precipitation in North China through East Asia–Pacific-North America wave trains (Ding and Liu 2001). When the Western North Pacific High moves northward, moisture from the mid-latitude Pacific Ocean becomes the main source of subtropical frontal precipitation (Lim et al. 2002).

4.2.1 India

The direct effect of orbital forcing enhances JJA precipitation in the Indian monsoon domain by ca 1.16 mm/day compared to present (Table 5, Fig. 5b, left) and ca 1.28 mm/day in the 5-member ensemble. The magnitude of the increase varies from model to model, ranging from 0.12 mm/day (GISS) to 2.37 mm/day (CNRM2). The increase in precipitation compared to today in the coupled PMIP2 OAGCM simulations is only 0.58 mm/day (Table 5,

Table 5 Change in simulated annual mean (ann) and summer (summ: June, July, August: JJA in northern hemisphere and December, January, February: DJF in southern hemisphere) precipitation for each model for each of the monsoon domains (Unit: mm/day)

Model			Northern Africa		Indian		East Asian		Southeast Asian	
Type	No.	Code	ann	summ	ann	summ	ann	summ	ann	summ
AGCM	1	BMRC	0.15	0.42	0.12	0.93	−0.39	−0.46	−0.49	−0.68
AGCM	2	CCC2	0.03	0.07	0.25	0.79	−0.02	0.19	−0.48	−0.49
AGCM	3	CCM3	0.09	0.26	0.19	1.03	0.01	0.31	0.15	0.14
AGCM	4	CCSR1	0.10	0.45	0.13	0.68	0.07	0.39	−0.06	0.10
AGCM	5	CNRM2	0.31	0.91	0.60	2.37	−0.04	−0.21	−0.43	−1.67
AGCM	6	CSIRO	0.04	0.10	0.21	0.61	0.03	0.38	−0.21	0.20
AGCM	7	ECHAM3	0.17	0.22	0.37	1.27	0.09	0.18	−0.26	−1.17
AGCM	8	GEN2	0.19	0.55	0.24	1.13	0.09	0.28	−0.27	0.08
AGCM	9	GFDL	0.22	0.70	0.43	1.41	−0.05	0.10	−0.21	−0.19
AGCM	10	GISS	0.06	0.26	−0.02	0.12	0.00	0.35	0.03	−0.14
AGCM	11	LMD4	0.12	0.80	0.55	1.89	−0.16	−0.39	0.00	−0.27
AGCM	12	LMD5	0.19	0.68	0.61	1.88	0.00	−0.04	−0.16	−0.22
AGCM	13	MRI2	0.07	0.49	0.49	1.69	−0.31	−0.31	−0.12	−0.39
AGCM	14	UGAMP	0.13	0.43	0.35	1.54	−0.10	−0.22	0.18	−0.28
AGCM	15	UIUC11	−0.05	−0.07	0.61	1.38	0.06	0.53	−0.29	−0.39
AGCM	16	UKMO	0.06	0.26	0.11	0.52	0.07	0.28	0.00	−0.01
AGCM	17	YONU	0.01	0.15	0.20	0.46	0.01	0.29	−0.11	0.10
		Mean	0.11	0.39	0.32	1.16	−0.04	0.10	−0.16	−0.31
		SD	0.09	0.27	0.20	0.60	0.13	0.31	0.20	0.49
OAGCM	1	CCSM	0.26	0.78	0.10	0.28	0.09	0.48	0.08	0.34
OAGCM	2	ECBILT	0.15	0.40	0.05	0.22	0.03	0.06	0.04	0.07
OAGCM	3	ECHAM5	0.31	0.70	0.19	0.45	0.01	0.38	0.07	0.32
OAGCM	4	FGOALS	0.55	1.42	0.05	0.54	−0.08	−0.20	−0.07	0.10
OAGCM	5	FOAM	0.15	0.55	0.06	0.50	−0.04	0.23	−0.04	0.26
OAGCM	6	GISS	0.49	1.14	0.11	0.49	0.04	0.24	0.12	0.44
OAGCM	7	HadCM3	0.38	1.02	0.22	0.93	0.12	0.53	0.29	0.93
OAGCM	8	IPSL	0.06	0.17	0.21	0.71	0.00	0.31	0.25	0.87
OAGCM	9	MIROC	0.35	0.90	0.26	0.88	−0.04	−0.06	0.15	0.54
OAGCM	10	MRI-fa	0.14	0.42	0.23	0.75	0.05	0.55	0.20	0.75
OAGCM	11	MRI-nfa	0.20	0.56	0.22	0.62	−0.03	0.33	0.11	0.45
		Mean	0.28	0.73	0.16	0.58	0.01	0.26	0.11	0.46
		SD	0.16	0.37	0.08	0.23	0.06	0.24	0.11	0.29

Model			North America		Southern Africa		Northern Australia		South America	
Type	No.	Code	ann	summ	ann	summ	ann	summ	ann	summ
AGCM	1	BMRC	−0.06	0.28	−0.04	−0.26	−0.02	−0.14	−0.22	−1.20
AGCM	2	CCC2	−0.08	−0.16	−0.43	−0.84	−0.24	−0.21	−0.20	−0.55
AGCM	3	CCM3	−0.06	0.12	−0.16	−0.87	−0.19	−0.72	−0.13	−1.02
AGCM	4	CCSR1	0.00	0.15	−0.11	−0.29	−0.09	−0.44	−0.16	−0.52
AGCM	5	CNRM2	−0.37	−0.84	−0.32	−1.04	−0.10	−0.31	−0.33	−0.29
AGCM	6	CSIRO	0.10	0.14	−0.23	−0.64	−0.52	−1.11	−0.17	−0.58
AGCM	7	ECHAM3	0.10	0.40	0.03	−0.14	−0.07	−0.28	−0.26	−1.02
AGCM	8	GEN2	0.17	0.19	−0.18	−0.46	−0.08	−0.69	−0.21	−0.80
AGCM	9	GFDL	−0.11	−0.04	−0.20	−0.68	−0.22	−0.84	−0.18	−1.02
AGCM	10	GISS	0.08	0.40	−0.19	−0.40	−0.06	−0.31	−0.01	−0.23
AGCM	11	LMD4	−0.12	−0.58	−0.12	−0.41	−0.22	−0.05	−0.19	−0.81

Table 5 continued

Model			North America		Southern Africa		Northern Australia		South America	
Type	No.	Code	ann	summ	ann	summ	ann	summ	ann	summ
AGCM	12	LMD5	−0.13	−0.56	−0.43	−1.05	−0.20	−0.41	−0.30	−0.73
AGCM	13	MRI2	0.10	0.30	0.04	0.13	−0.33	−1.11	−0.05	−0.42
AGCM	14	UGAMP	−0.14	−0.25	−0.12	−0.18	−0.20	−0.43	−0.16	−0.95
AGCM	15	UIUC11	−0.04	0.02	−0.25	−0.41	−0.29	−1.28	−0.15	−0.88
AGCM	16	UKMO	0.02	0.11	−0.22	−0.73	−0.14	−0.72	−0.08	−0.28
AGCM	17	YONU	0.13	0.60	−0.18	−0.42	−0.09	−0.72	0.06	−0.54
		Mean	−0.02	0.02	−0.18	−0.51	−0.18	−0.58	−0.16	−0.70
		SD	0.13	0.39	0.13	0.33	0.12	0.36	0.10	0.30
OAGCM	1	CCSM	0.13	0.40	−0.02	−0.24	−0.13	−0.54	−0.13	−0.52
OAGCM	2	ECBILT	0.06	0.20	0.02	−0.19	0.03	−0.14	0.01	−0.13
OAGCM	3	ECHAM5	0.05	0.09	−0.09	−0.33	−0.18	−0.39	−0.11	−0.33
OAGCM	4	FGOALS	0.24	0.52	−0.10	−0.55	−0.28	−0.91	−0.20	−0.53
OAGCM	5	FOAM	0.15	0.38	0.03	−0.09	−0.04	0.07	−0.27	−0.67
OAGCM	6	GISS	0.06	0.22	−0.05	−0.14	−0.11	−0.52	−0.08	−0.40
OAGCM	7	HadCM3	−0.02	0.06	−0.14	−0.45	−0.04	−0.68	−0.26	−1.11
OAGCM	8	IPSL	−0.04	−0.17	−0.15	−0.33	0.02	−0.05	−0.11	−0.30
OAGCM	9	MIROC	−0.03	0.05	−0.07	−0.06	−0.12	−0.34	−0.10	−0.55
OAGCM	10	MRI-fa	0.05	0.21	−0.14	−0.30	−0.09	−0.44	−0.08	−0.33
OAGCM	11	MRI-nfa	0.10	0.30	−0.14	−0.33	−0.13	−0.46	−0.15	−0.50
		Mean	0.07	0.21	−0.08	−0.27	−0.10	−0.40	−0.14	−0.49
		SD	0.08	0.19	0.06	0.15	0.09	0.28	0.08	0.25

Fig. 5b, right) in the full ensemble, and only 0.64 mm/day in the 5-member ensemble; the inter-model variation is also smaller, ranging from 0.22 mm/day (ECBILT) to 0.93 mm/day (HADCM3). The difference between the two sets of simulations is significant at the 99% level (Table 6). Thus, ocean feedback appears to damp the response of the Indian monsoon to orbital forcing.

The PMIP1 AGCM simulations are characterised by a strengthening (relative to the control) of the thermal low over Eurasia (2.5 h/Pa), resulting in increased onshore flow into the Indian subcontinent. The strengthening of the thermal low is a direct consequence of the orbitally-induced increase in summer temperature over the northern hemisphere land masses (Table 4). The Mascarene High is slightly weaker (-0.2 h/Pa) than in the control simulations because of the increased SH insolation during austral winter. Thus, changes in the Indian monsoon at 6 ka appear to be a response to local (northern tropical) changes and not due to changes in the strength of cross-equatorial flow. The strengthening of the Eurasian thermal low compared to present is greater in the coupled 6 ka simulations (3.0 h/Pa), and again the Mascarene High is somewhat weaker (−0.2 h/Pa) than today. SSTs in the Arabian Sea are ca 0.9°C lower than today in late spring (April, May) and remain lower until August (Fig. 6). The lower SSTs minimize moisture supply during most of the Indian monsoon season (June to September). At the same time, SSTs over the western tropical North Pacific are slightly higher than today in September. This results in the deepening of the low pressure cell in this region at a time when the Eurasian thermal low is weakening. This change results in more moisture convergence over the western tropical North Pacific, hence further reducing onshore flow into the Indian subcontinent. Thus, the reduction in the strength of the Indian monsoon at 6 ka in the PMIP2 OAGCM experiments appears to result from the combined effect of changes in SSTs over both the Arabian Sea and the western tropical North Pacific.

Previous studies (e.g. Hewitt and Mitchell 1998; Braconnot et al. 2000; Voss and Mikolajewicz 2001; Liu et al. 2004; Ohgaito and Abe-Ouchi 2007; Marzin and Braconnot 2009) are equivocal about the impact of ocean feedback on the Indian monsoon. Liu et al. (2004) suggested that ocean feedback reduced precipitation over the Indian subcontinent, as in our analyses and those of Voss and Mikolajewicz (2001), Ohgaito and Abe-Ouchi (2007) and Marzin and Braconnot (2009), but Hewitt and Mitchell (1998) implied that feedback resulted in increased monsoon precipitation. This difference is in part due to differences in the definition of the region affected by the

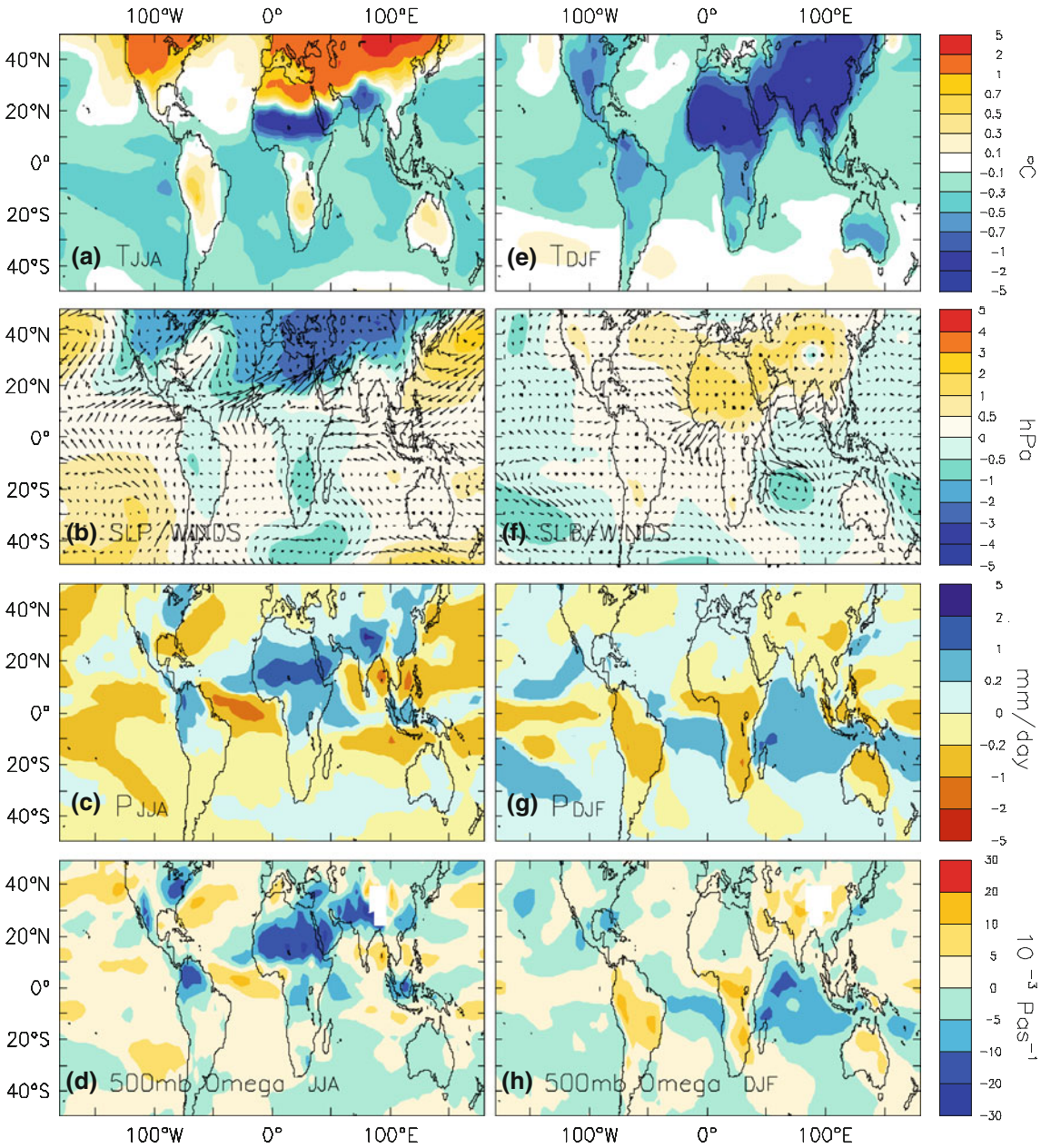

Fig. 4 Changes in climate between 6 ka and present day, based on the difference between the 11-model ensemble mean of the OAGCM control and 6 ka climate simulations: **a** surface temperature (°C) during boreal summer/austral winter (June, July, August: JJA), **b** sea level pressure (hPa) and surface wind patterns during boreal summer/austral winter, **c** 500 mb vertical velocity, omega (10^{-3} Pa/s) during boreal summer/austral winter, **d** precipitation (mm/day) in boreal summer/austral winter, **e** surface temperature (°C) during boreal winter/austral summer (December, January, February, DJF), **f** sea level pressure (hPa) and surface wind patterns during boreal winter/austral summer, **g** 500 mb vertical velocity, omega (10^{-3} Pa/s) during boreal winter/austral summer, **h** precipitation (mm/day) in boreal winter/austral summer

monsoon: Liu et al. (2004) presented averages for the region 10–40°N, 60–110°E (which includes the Indian subcontinent and part of East Asia) while Hewitt and Mitchell (1998) used the region 7.5–30°N 67.5–127.5°E (which includes a much larger part of Southeast Asia). Using the Liu et al. (2004) definition, we obtain an increase of 0.78 mm/day compared to present for the ensemble of PMIP1 AGCM simulations and of only 0.43 mm/day from the ensemble of PMIP2 OAGCM simulations. However, using the Hewitt and Mitchell (1998) definition, we obtain increases of 0.28 mm/day for the PMIP2 AGCM simulations and 0.46 mm/day for the PMIP2 OAGCM simulations. Precipitation is reduced by ca 0.31 mm/day over Southeast Asia (7.5–30°N, 105–127.5°E) in the PMIP1

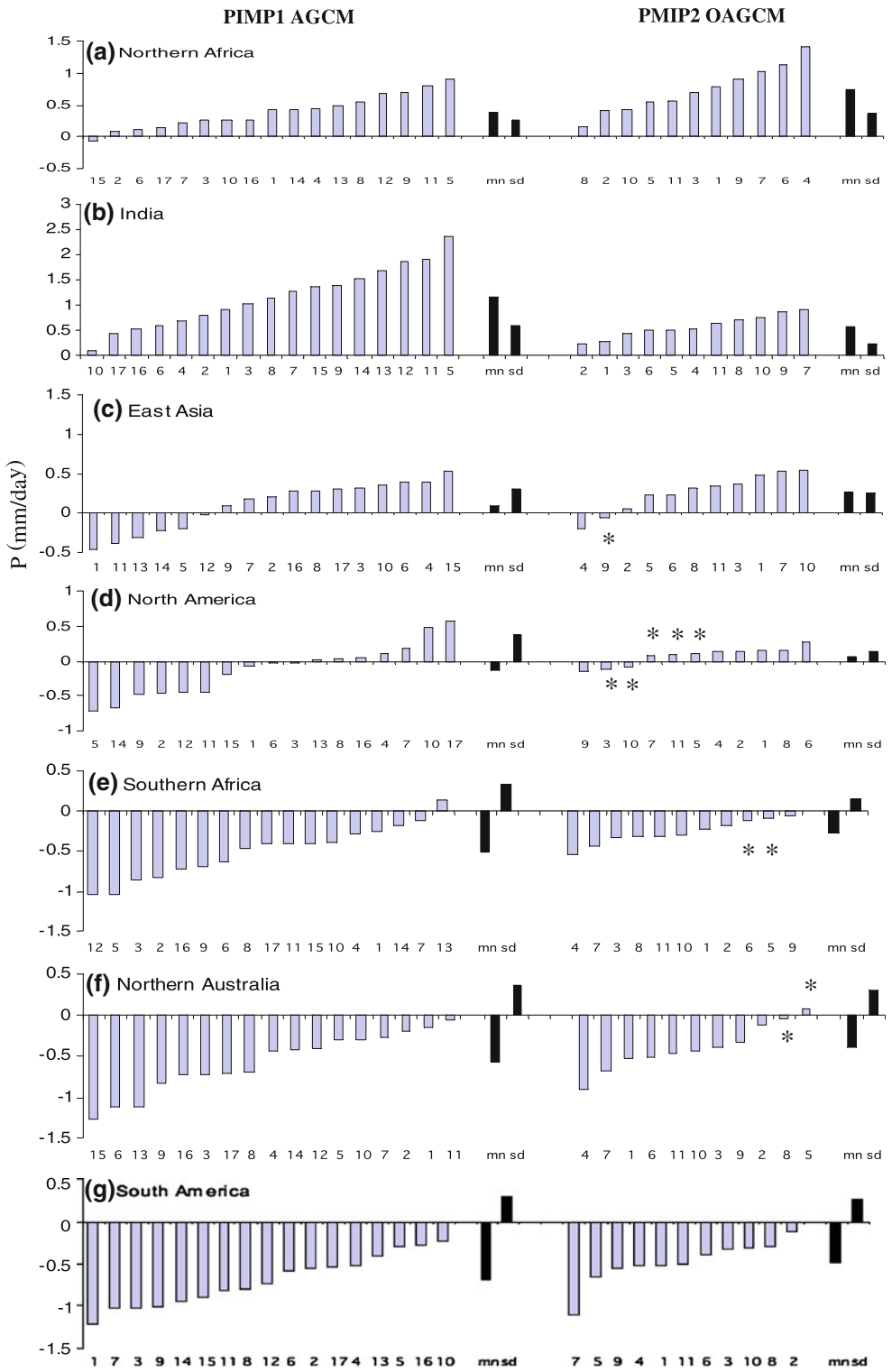

Fig. 5 Summer monsoon precipitation changes shown by individual PMIP1 AGCM (*left column*) and PMIP2 OAGCM (*right column*) models over **a** northern African monsoon (12–30°N, 20°W–30°E), **b** Indian monsoon (20–40°N, 70–100°E), **c** East Asia monsoon (20–50°N, 100–150°E), **d** North America monsoon (20–40°N, 95–120°W and 0–20°N, 60–120°W), **e** southern Africa monsoon (5–35°S, 0–50°E), **f** northern Australia monsoon (5–25°S, 110–150°E) and **g** South America monsoon (5–25°S, 30–70°W). The ensemble mean (mn) and the inter-model standard deviations (SD) are indicated in the last two columns at each group. The boreal summer monsoon (**a**–**d**) is JJA seasonal mean and the austral summer monsoon (**e**–**g**) is DJF seasonal mean. The *numbers* at the foot of each column indicate the model represented and can be found on Tables 4 and 5. The signals of *star* (*) indicate the changes in regional mean of summer precipitation simulated by the corresponding OAGCM are not significant at the 95% level

Table 6 Significance of differences in simulated precipitation between the PMIP1 AGCM and PMIP2 OAGCM simulations for each of the monsoon regions, where *** indicates significant at the 99% level, ** indicates significant at the 95% level, and * indicates significant at the 90% level

Monsoon region	PMIP1 AGCM		PMIP2 OAGCM		*T* test
	Mean	SD	Mean	SD	
Northern Africa	0.39	0.27	0.73	0.37	2.70 ***
Indian	1.16	0.60	0.58	0.23	−2.95 ***
East Asian	0.10	0.31	0.26	0.24	1.40
Southeast Asia	−0.31	0.49	0.46	0.29	−2.99 ***
North America	0.02	0.39	0.21	0.19	1.45
North America (minus IPSL)	0.02	0.39	0.39	0.24	2.01**
Southern Africa	−0.51	0.33	−0.27	0.15	2.16 **
Northern Australia	−0.58	0.36	−0.40	0.28	1.33
South America	−0.70	0.30	−0.49	0.25	1.86*

Results are given for the North American monsoon region both including and excluding the IPSL model, which has a significant cold bias over the tropical eastern Pacific

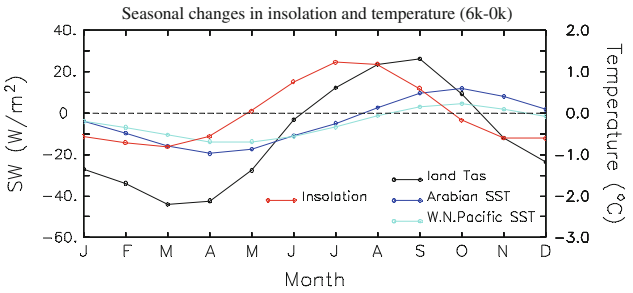

Fig. 6 Relationships between the seasonal cycle of insolation over northern tropics (20–40°N), sea-surface temperatures in the Arabian Sea (55–75°E, 5–15°N; Arabian SST), the western tropical north Pacific (110–160°E, 0–20°N; W.N.Pacific SST), and temperature changes over Indian monsoon region (60–100°E, 20–40°N; land Tas)

AGCM simulations and increased by ca 0.46 mm/day in the PMIP2 OAGCM simulations. Thus, the response of the Southeast Asian monsoon to ocean feedback is to strongly enhance monsoon rainfall in this area compared to present, and inclusion of a substantial area of Southeast Asia in the estimation of a regional average will lead to erroneous conclusions about the impact of ocean feedback on the Indian monsoon. Both Liu et al. (2004) and Hewitt and Mitchell (1998) recognised that precipitation was increased over Southeast Asia and attributed this to increased low-level moisture convergence as a result of warmer SSTs in the western tropical North Pacific.

Braconnot et al. (2000), in simulations made with an earlier version (IPSL-CM1) than the version included in the PMIP2 database (IPSL-CM4), found that ocean feedback substantially enhanced monsoon precipitation in northern India. This resulted from strengthened and more southeasterly convection caused partly by a strengthening of the Eurasian low (4 hPa higher than the atmosphere-only simulation) and partly by the formation of an extremely deep low pressure system (6 hPa lower than the atmosphere-only simulation) localised at the foot of the Himalyas (ca 32°N, 82°E). This localised low pressure is not seen in the current version of the IPSL model and the increase in the strength of the Eurasian low (compared to the control) is only 2 hPa, and lies in the middle range of the changes shown by the ensemble of PMIP2 OAGCM experiments. The difference in the strength of the Eurasian low between the PMIP1 AGCM and PMIP2 OAGCM simulations is much smaller (<1 hPa, Figs. 3b, 4b), and as a result the increase in convection is negligible and far outweighed by the reduction in precipitation caused by lower SSTs in the Arabian Sea. It is not possible to diagnose the cause of the very different response of the Indian monsoon to ocean feedback shown in the early version of the IPSL model because of the substantial differences to atmospheric, land-surface and oceanic components between the two versions. However, the occurrence of a highly localised low pressure cell in the IPSL-CM1 version does suggest that the response of the Indian monsoon to orbital forcing and ocean feedback may be sensitive to land-surface parameterisations.

Our analyses indicate that ocean feedback reduces the response of the Indian monsoon to orbital forcing. A similar result has been found by Liu et al. (2004), Voss and Mikolajewicz (2001), Ohgaito and Abe-Ouchi (2007) and Marzin and Braconnot (2009). Ohgaito and Abe-Ouchi (2007) showed that the reduction is linked to changes in ocean thermodynamics. Liu et al. (2004) and Marzin and Braconnot (2009) suggested a further mechanism, specifically the strengthening of convection over the western tropical North Pacific which reduces moisture flow into India continent. In our analysis, lower SSTs in the Arabian Sea during spring and summer also lead to a reduction in the primary source of moisture supplying the Indian monsoon. The role of changes in SSTs in the Arabian Sea has not been recognised previously.

4.2.2 *East Asia*

The response to the direct effect of orbital forcing in the PMIP1 AGCM simulations (Table 5, Fig. 5c, left) over East Asia is variable: 11 models produce an increase in summer precipitation but 6 models show reduced rainfall at 6 ka compared to present. The change in precipitation ranges from a decrease of -0.46 mm/day (BMRC) to an increase of 0.53 mm/day (UIUC11). Although the ensemble response indicates increased precipitation

(0.10 mm/day, 0.08 mm/day in the 5-member ensemble), this is much less than the inter-model variance (0.31 mm/day). In the PMIP2 OAGCM simulations (Table 5, Fig. 7a, right), 9 out of the 11 models show a statistically significant increase in precipitation compared to present, but FGOALS produces a significant decrease (−0.20 mm/day) in rainfall over this region. (The small decrease in precipitation shown by MIROC is not statistically significant.) The ensemble response is an increase of 0.26 mm/day, similar to the inter-model variance (0.24 mm/day) although the increase in the 5-member ensemble is larger (0.45 mm/day). Given the large inter-model variances in both sets of simulations, the change resulting from ocean feedback is not registered as significant (Table 6). There is a shift in the timing of peak monsoon rainfall between the PMIP1 AGCM (not shown) and PMIP2 OAGCM (not shown) simulations: the peak occurs in June in the PMIP1 AGCM simulations and in July in the PMIP2 OAGCM simulations. In the PMIP2 OAGCM simulations, mean precipitation in July–August-September (JAS) is increased by 10% compared to today over northern China (35–50°N, 100–130°E) but only by 6% over southern China (20–35°N, 100°–130°E). This reflects the fact that the monsoon front lies to the north of its modern position. Thus, ocean feedback affects both the location and the timing of peak monsoon rainfall in the East Asian sector.

The inter-model differences in the response to orbital forcing in both the PMIP1 AGCM and PMIP2 OAGCM simulations reflect the portrayal of the dynamical structure of the East Asian monsoon in the control simulations (see e.g. Fig. 7, left column). Convection is strongly developed over the Southeast Asia/South China Sea region (5°S–20°N), with wind convergence near the surface and divergence aloft (200 hPa). This strong rising motion is to some extent compensated by subsidence in the SH (5°S–20°S). Descending motion can also be identified in the subtropics, but the exact location varies from model to model. It is farthest to the south in FGOALS (20–25°N) and occurs at ca 25–30°N in CCSM, 30–35°N in FOAM, 35–40°N in GISS, 30–40°N in MRI-fa and MRI-nfa and 40–50°N in MIROC. This downward motion grossly corresponds to upper-level wind convergence and near-surface divergence (i.e. from the Western North Pacific High). Although all the models reproduce the dynamical structure of the East Asian monsoon, the differences in the location (and intensity) of the Western North Pacific High has a significant effect on the location of precipitation in the East Asian sector.

At 6 ka, all the models show an increase (compared to the control simulations) in the strength of upward motion at the equator (Fig. 7, right column) where SSTs in the late summer are warmer than today. Enhanced convection over warmer SSTs pushes the Western North Pacific High further north, leading to the formation of a pronounced wave train from 10°N to 60°N (seen most clearly at the 200 mb level). As a result of tropical SSTs being higher than in the control simulations, more moisture is transported by the southerly winds into China. Moisture transport from the Western North Pacific by the easterly component of the southeast flank of Western North Pacific High is also enhanced. SSTs in the Western North Pacific (Fig. 6) are higher than present through the autumn (September to November), and this contributes to lengthening the monsoon season and thus to the shift in peak monsoon rainfall between the PMIP2 OAGCM and PMIP1 AGCM simulations in the East Asian monsoon sector.

In a recent study using the IPSL-CM4, Marzin and Braconnot (2009) found that ocean-feedback reduced East Asian precipitation significantly. Our analyses suggest that this conclusion is likely model-dependent: there is no consistency between models, either with respect to the direct impact of orbital forcing or the strength of the ocean-feedback on East Asian rainfall. State-of-the-art OAGCMs do not reproduce the distribution and magnitude of summer precipitation in the East Asian monsoon region today particularly well (Zhao et al. 1995; Christensen et al. 2007).

4.3 North America

In response to the Northern Hemisphere summer insolation maximum, the American continent warms, and the region from the equator northward through Central America and into the northern mid-latitudes has a summer precipitation maximum. The North American summer monsoon (Adams and Comrie 1997; Vera et al. 2006) and the associated Mexican monsoon (Douglas et al. 1993) are a response to heating on the Colorado Plateau and the Central American highlands, with upper-troposphere divergence, low-level convergence and concomitant focusing of precipitation. The thermally-induced high pressure in southwestern North America is associated with northward movement of the Pacific and Bermuda high pressure systems and the formation of southerly low-pressure jets over the Gulf of California. Low-level moisture transport occurs through boundary level flow from the Gulf of California, with an additional moisture source from middle tropospheric southeasterly flow from the Gulf of Mexico (Vera et al. 2006). Nevertheless, in part because of the more limited area of land involved, the absolute amount of summertime precipitation associated with the North American monsoons are substantially less than the precipitation associated with other northern hemisphere monsoons. Monsoon rains in the American Southwest and Central America are associated with drier conditions in the Pacific Northwest, the northern Great Plains, and the mid-continent due to the

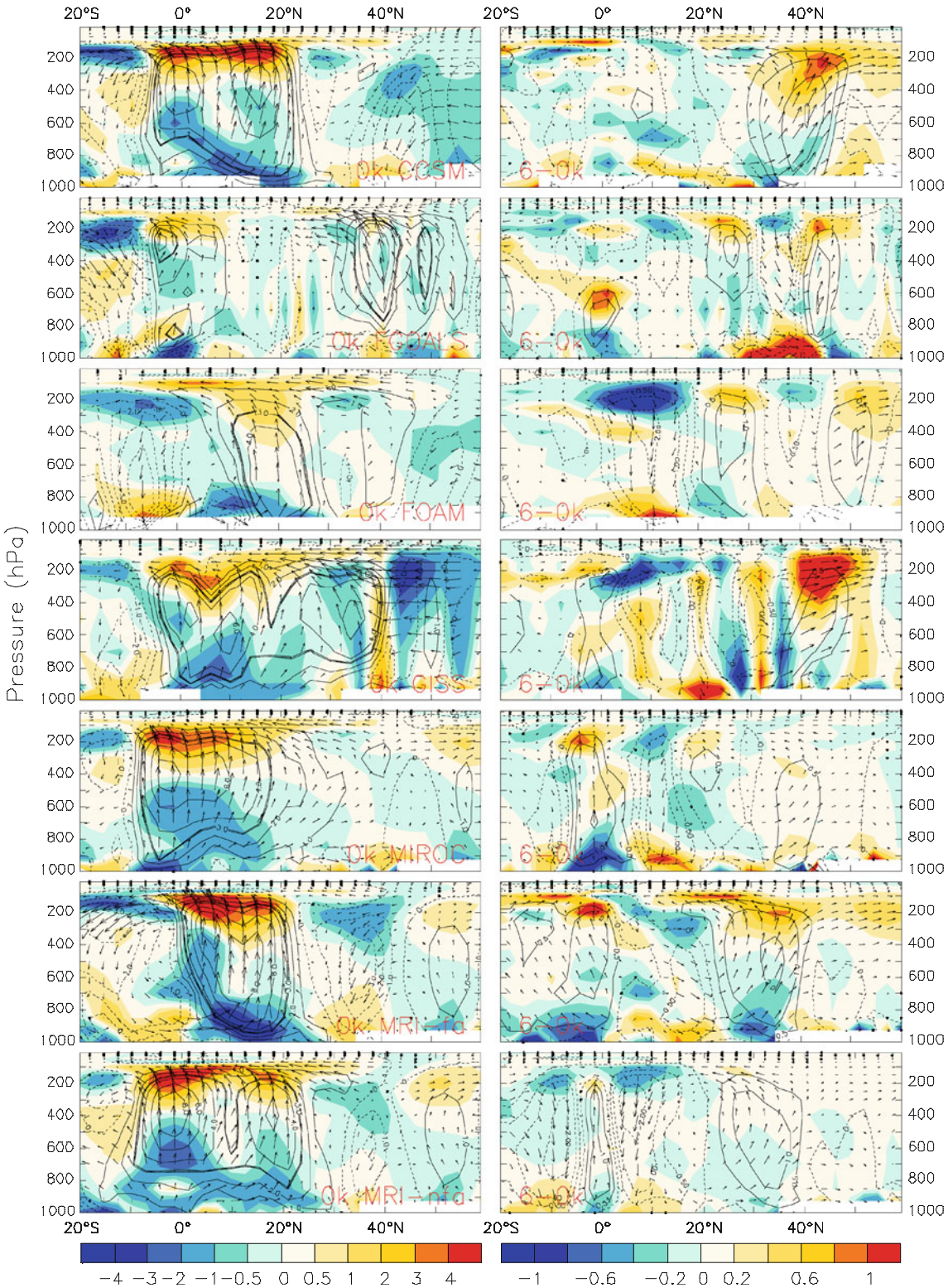

Fig. 7 Latitude-pressure longitude-mean (110°E–130°E) cross section of horizontal divergence ($\partial u/\partial x + \partial v/\partial y$, in color) and meridional flow (vertical flow is amplified by a factor of 100) over the Asian monsoon sector during July–August for individual models. *Left column* shows the control simulations (0 k); right column shows difference between the mid-Holocene and control simulations (6-0 k). The *contour* is vertical velocity. *Solid lines* indicate upward motion, and *dashed lines* downward motion. The *contour line* is from −0.05 to 0.05 ($\times 10^{-3}$) Pa/s

formation of a crescent-shaped region of enhanced subsidence bordering the area of the enhanced monsoon (Higgins and Shi 2000). In response to the wintertime insolation minimum, the North American continent cools and the storm tracks shift southward. Over eastern and central North America, the prevailing wind direction switches from south in summer to north in winter. These changes in temperature, storm tracks, and prevailing wind direction are manifestations of the Northern Hemisphere American winter monsoon, and account for winter precipitation maxima along the west coast of North America.

Direct insolation forcing produces an increase in precipitation over the southwestern USA and northernmost South America, but precipitation over central America is reduced in the AGCM simulations. As a result, precipitation over the region as a whole is only increased by 0.02 mm/day in the PMIP1 AGCM experiments (and 0.07 mm/day in the 5-member ensemble) compared to present. However, there are large differences between model estimates of the change in precipitation in the PMIP1 AGCM experiments (Fig. 5d, left) ranging from −0.84 mm/day (CNRM-2) to 0.60 mm/day (YONU). There is more consistency amongst the PMIP2 OAGCM experiments (Fig. 5d, right): all but one model (IPSL) register increased precipitation over the domain as a whole, ranging from 0.06 mm/day (HADCM3) to 0.52 mm/day (FGOALS). The reduction in precipitation shown by the IPSL model (−0.17 mm/day) is probably a consequence of the cold bias over the tropical oceans (and particularly the tropical Pacific) in this model. Thus, ocean feedback produces a general increase in precipitation (ca 0.21 mm/day, though only 0.12 mm/day in the 5-member ensemble) compared to present in the American NH monsoon region. The impact is most noticeable over Central America, where precipitation increases by ca 0.10 mm/day in the PMIP2 OAGCM simulations. When IPSL is excluded from consideration, the difference between the PMIP1 AGCM and PMIP2 OAGCM simulations is significant at the 95% level (Table 6).

Increased NH summer insolation at 6 ka results in an increase in temperature by ca 1°C compared to present over North America (ca 0.55°C over the domain as a whole: Table 4) solely as a response to the direct orbital forcing, leading to a deepening of the thermal low over the continent (by ca 1.0 h/Pa) and intensified onshore flow. As a result precipitation is enhanced compared to present over the American Southwest USA (Fig. 3a–c). The response is similar, though more muted, in northern South America: the moderate strengthening of the thermal low (by ca 0.2 h/Pa) in response to the increase in summer insolation results in enhanced monsoon precipitation. The change in temperature over Central America in response to orbital forcing alone is negligible because of the small area of land involved, and as a result precipitation is somewhat reduced compared to present in this region. The warming over North America is ca 1.4°C in the coupled PMIP2 OAGCM simulations and as a result the thermal low is strengthened (compared to the PMIP1 AGCM simulations) and southwesterly surface winds are further intensified (compared to the AGCM simulations), enhancing low-level moisture transport from the tropical eastern Pacific into the American Southwest (Fig. 8). However, the main impact of ocean feedback on the American monsoon is related to a steepening of the SST gradient across in the low latitudes, caused by lower temperatures in the equatorial oceans and increased temperatures in the mid-latitudes (Fig. 4a). Lower SSTs result in increased sea-level pressure in the equatorial zone, while increased SSTs over the mid-latitude oceans results in the weakening and northward displacement of both the Pacific and Atlantic subtropical highs. In the Pacific sector, the steepened SST gradient results in strengthened onshore flow and enhanced precipitation over both the American Southwest and Central America. In the Atlantic, the weakened subtropical high is also centred further west than in the control simulations as a result of the enhanced thermal low over northern Africa (Fig. 4). This leads to enhanced moisture convergence over the Caribbean, a further factor contributing to the very large enhancement of precipitation in Central America in the PMIP2 OAGCM simulations. Enhanced low-level moisture convergence into the monsoon core regions in these simulations results in increased convective instability and hence increased uplift, and is accompanied by a corresponding increase in subsidence (and hence increased aridity) in the regions surrounding the monsoon core.

Our results are broadly consistent with analyses of the impact of orbital forcing and ocean feedback on the NH American monsoon made by Harrison et al. (2003; results also discussed in Liu et al. 2004). Although it is clear that the magnitude (and exact location) of the change in monsoon precipitation varies somewhat from model to model, the general mechanisms are robust. Specifically, our analyses confirm that ocean feedback enhances monsoon precipitation in the American Southwest and is crucial for the development of an enhanced monsoon in Central America. While Harrison et al. (2003) emphasised the role of the strengthening of the SST gradient (cool equator/warm mid-latitudes) in the North Pacific on this enhancement, we suggest that changes in the Atlantic may have been equally important. The easterly anomaly over the western tropical Atlantic in the FOAM model is relatively weak compared to the other PMIP2 models, and this may explain why the role of changes in the Atlantic was not emphasised in the Harrison et al. (2003) analyses.

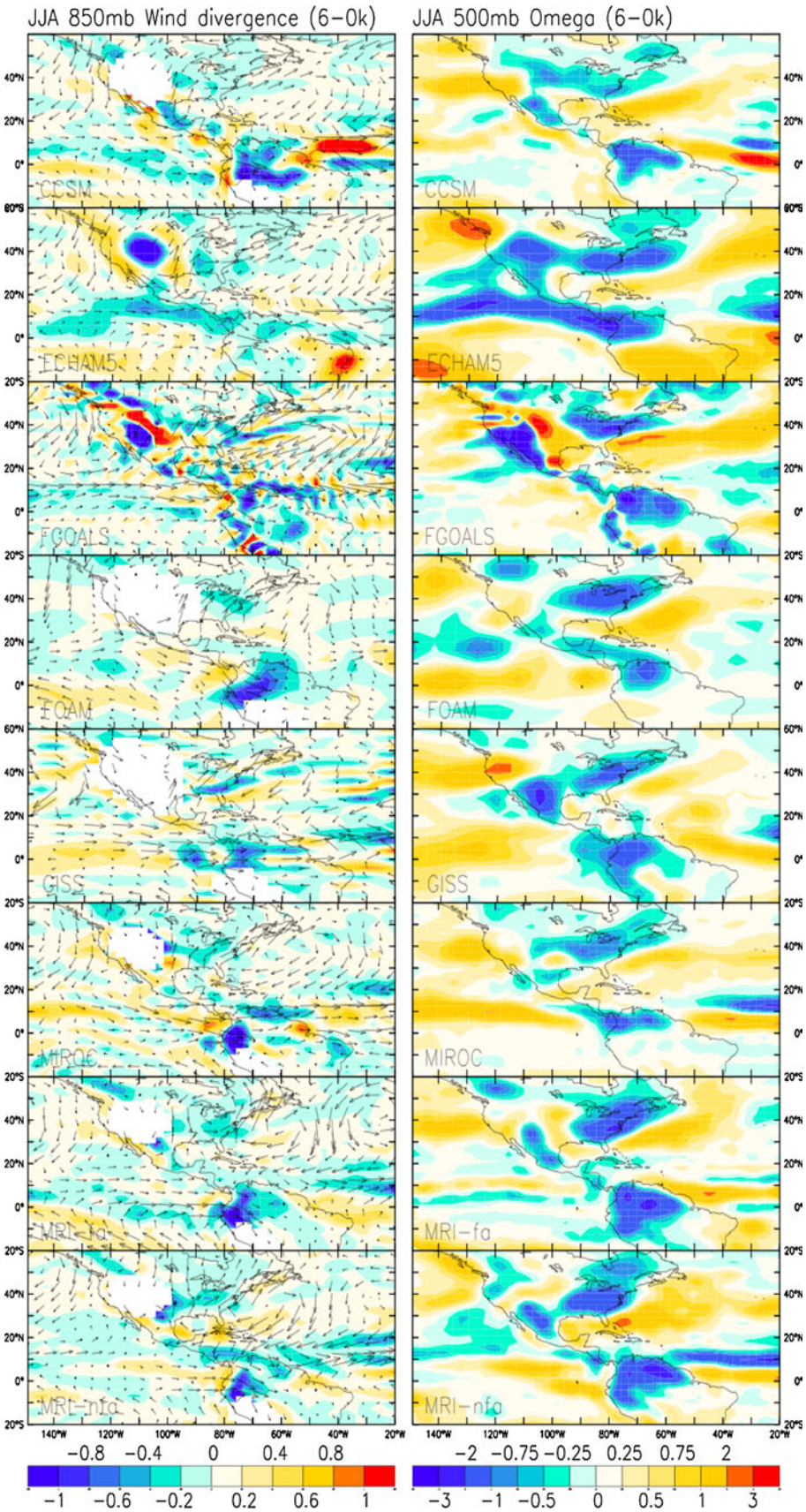

Fig. 8 Changes in climate between 6 ka and present day over North American monsoon region during boreal summer (JJA) for individual models. *Left column* shows 850-mb wind divergence (in *color*) and surface wind patterns; *right column* shows 500 mb vertical velocity, omega (10^{-3} Pa/s), down is positive

4.4 Southern Africa

The mean decrease in southern Africa monsoon precipitation (compared to present) in the PMIP1 AGCM simulations is −0.51 mm/day (Fig. 5e left, Table 5) and −0.53 mm/day in the 5-member ensemble. The decrease (compared to present) is smaller in the PMIP2 OAGCM simulations: −0.27 mm/day (Fig. 5e right, Table 5) in the full ensemble and −0.33 mm/day in the 5-member ensemble. The difference between the two sets of simulations is significant at the 95% level (Table 6).

The direct radiation effect weakens the southern African monsoon in general (Fig. 3). In summer (DJF) the temperature over the southern part of the continent is lowered (Fig. 3d) by ca −0.55°C, SLP over the land is increased, leading to reduced surface inflow (Fig. 3e) and, as a result, a reduction in precipitation (Fig. 3f). The reduction in precipitation is most marked in the eastern part of the region, suggesting a significant truncation of eastward penetration of rain-bearing winds. In the PMIP2 OAGCM experiments (Fig. 4), the decrease in temperature over the continent is somewhat greater (−0.60°C) in the PMIP2 OAGCM experiments (Fig. 4) than in the PMIP1 AGCM simulations. However, the equatorial and subtropical Atlantic is also colder. There is no significant change in SLP over the continent, and onshore flow is more marked than in the PMIP1 AGCM simulations, resulting in a weaker reduction in precipitation compared to present than shown in the PMIP1 AGCM simulations. The reduction in precipitation is relatively homogeneous across the continent, and this helps to explain why the difference between the two sets of simulations is so large.

Our results confirm Liu et al. (2004)'s conclusions that the southern African monsoon is weaker than today during the mid-Holocene as result of reduced summer insolation and that ocean feedbacks mitigate the orbitally-induced suppression of the South African monsoon to some extent, resulting in a slightly less pronounced reduction in precipitation compared to toady. Liu et al. (2004) highlighted the role of warmer-than-present waters off the southwestern coast of Africa and weakening of the sub-tropical high pressure cell in mitigating the orbitally-induced weakening of the southern African monsoon, in large part because the largest changes shown in that simulation occurred south of 20°S. Nevertheless, the Liu et al. (2004) simulations also show the increased onshore flow due to ocean feedback invoked here to explain differences between the two sets of PMIP simulations.

4.5 Northern Australia

Rainfall over northern Australia is highly seasonal, with over 90% of the annual precipitation occurring between November to April (Nicholls et al. 1982). As with other monsoon systems, the Australian summer monsoon is associated with seasonal insolation changes which lead to increased surface temperature over the Australian continent and the formation of a thermal (Kullgren and Kim 2006). Increased surface warming in conjunction with the anomalous cyclonic circulation, produces increased moisture convergence over the continental interior. In conjunction with the anomalous cyclonic circulation, zonal wind anomalies over northern Australia change from easterly to westerly. The main source of moisture is northwesterly flow from the Banda and Coral Seas. Nevertheless, the Australian monsoon is anomalous because of the degree to which it is influenced by cross-equatorial airflows and hence can be influenced by NH conditions (Trenberth et al. 2000). In NH autumn and winter, the ITCZ moves from the NH to the SH. There is strong atmospheric convergence associated with the southerly position of the ITCZ in Austral summer. At low levels, the dry southeasterly trades are displaced poleward as equatorial westerlies bring moisture into a region of cyclonic vorticity—the monsoon trough—over northern Australia. Thus, Australian monsoon rainfall is a combination of north–south seasonal displacements of the ITCZ in the Indonesian region, together with an essentially east–west monsoonal circulation.

The direct radiation effect decreases Northern Australian monsoon precipitation by ca −0.58 mm/day compared to present (Fig. 5f, left, Table 5) and ca −0.65 mm/day in the 5-member ensemble; the reduction in the coupled PMIP2 OAGCM experiments (compared to present) is −0.40 mm/day (Fig. 5f, right, Table 5) and −0.42 mm/day in the 5-member ensemble. Thus, the oceanic feedback appears to minimize the orbitally-induced reduction of precipitation. There is a considerable range in the magnitude of the simulated reduction in the PMIP1 AGCM experiments, from −0.05 mm/day (LMD4) to −1.28 mm/day (UIUC11). The range is similarly large in the PMIP2 OAGCM simulations (Table 5), and indeed one model (FOAM) produces a slight increase in precipitation as a result of ocean feedback.

As a result of reduced insolation in summer (DJF), temperatures over the Australian continent are lower than today (Fig. 3d). The maximum cooling is registered in the southern part of the continent, where summer temperatures are >−0.7°C lower than in the control simulation. The thermal low over central Australia (Fig. 3e) is less deep (by ca 1.0 hPa) and this results in reduced surface inflow (Fig. 3e). Precipitation is reduced by ca 0.6 mm/day over the continent as a whole (Fig. 5) and by >1.0 mm/day over northeast Australia (Fig. 3f). In the coupled OAGCM experiments, the decrease in temperature over southern Australia compared to present is somewhat smaller

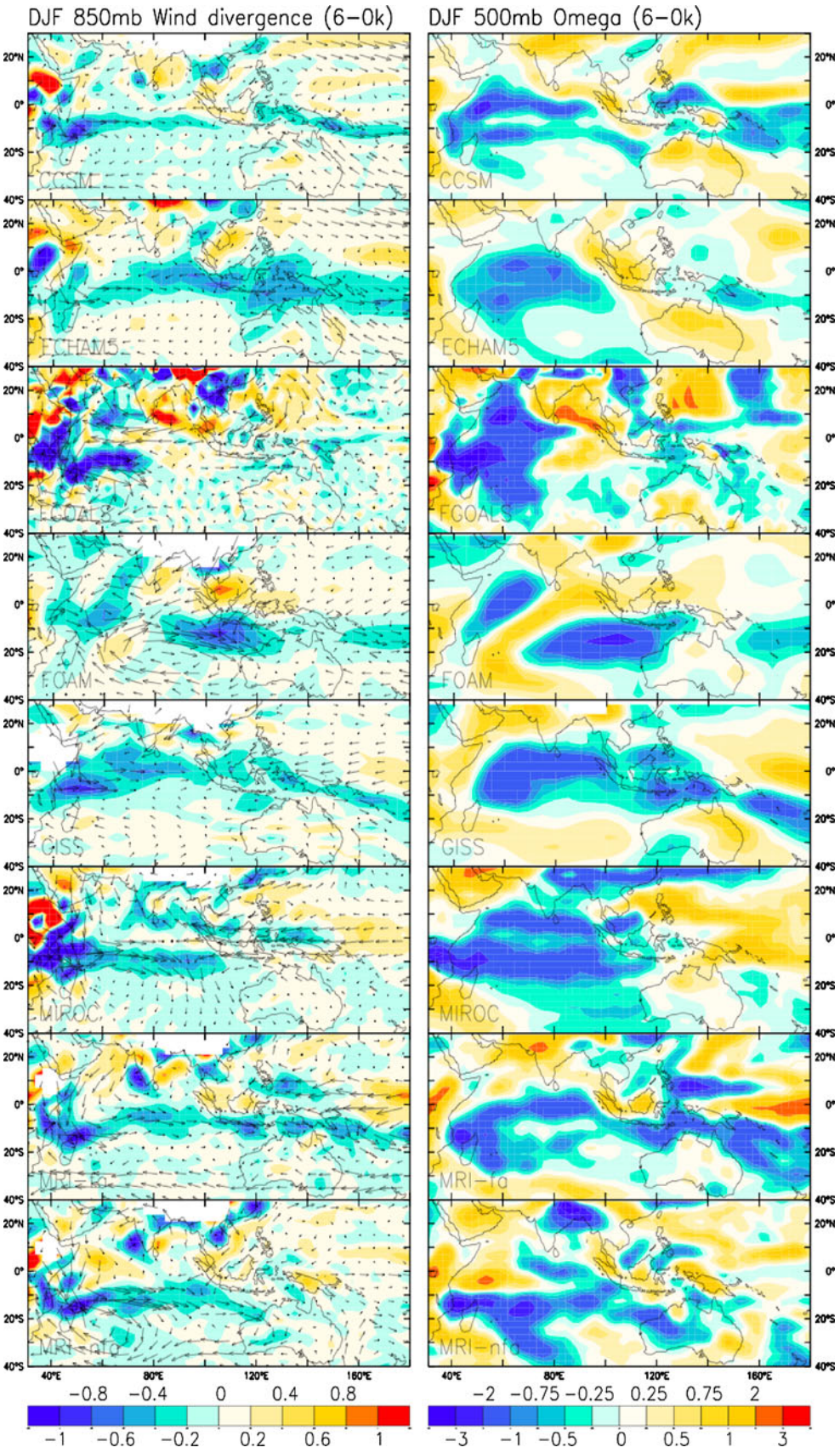

Fig. 9 Changes in climate between 6 ka and present day over Asian–Australian monsoon region during austral summer (DJF) for individual models. *Left column* shows 850-mb wind divergence (in *color*) and surface wind patterns; *right column* shows 500 mb vertical velocity, omega (10^{-3} Pa/s), down is positive

(<−0.7°C) (Fig. 4e). The thermal low is less deep than today (by ca 0.5 hPa) (Fig. 4f) and surface inflow is correspondingly reduced (Fig. 4f). Thus, ocean feedback mitigates the direct effects of orbital forcing and the overall reduction in monsoon precipitation is ca 0.4 mm/day over the continent as a whole (Fig. 7) and <1.0 mm/day over northeast Australia (Fig. 4e). These changes can be seen as a purely thermal response, caused by the buffering effect of the warm oceans. Ocean feedback also affects the Australian monsoon through changing the location of moisture convergence. Ocean feedback results in the strengthening of the monsoon trough in the tropical western Pacific (Fig. 4f), resulting in increased cross-equatorial flow both from the Indian Ocean via the tropical South Indian Ocean (Fig. 9, left column) and from the tropical west Pacific via the South China Sea (Fig. 9, left column) and convergence of moisture-laden airflow over northern Australia and New Guinea. The strength of cross-equatorial flow is governed by the enhanced Asian winter monsoon (Fig. 3). The Pacific trade winds are also enhanced, bringing additional moisture from the central Pacific into the tropical western Pacific.

According to Liu et al. (2004), while orbital forcing produced a reduction in the Australian monsoon, ocean feedbacks produced an overall enhancement in monsoon precipitation during the mid-Holocene compared to present. A more recent study, again with the FOAM model, has also shown an overall enhancement in mid-Holocene precipitation over northern Australia (Marshall and Lynch 2006). Our analyses suggest that this response is not typical of coupled OAGCMs: in our analyses, FOAM is the only model that produces an increase in precipitation (0.07 mm/day) compared to today in response to the combined effect of orbital forcing and ocean feedback. The response here is smaller than the 0.52 mm/day reported by Liu et al. (2004). There may be several reasons for this difference, including changes in model configuration and differences in analytical techniques. In our analysis, we have estimated changes in monsoon precipitation only over land areas and have defined model gridcells as land when more than 70% of the gridcell area is occupied by land. We cannot ascertain how land areas were defined in Liu et al. (2004), but sensitivity tests show that including all grid cells that contain some percentage of land leads to increases in the area-averaged change in precipitation. For example, including all grid cells that include any area of land would increase the simulated change in monsoon precipitation from the 0.07 mm/day reported here to 0.30 mm/day.

Liu et al. (2004) showed that the response in the FOAM model was caused by a combination of remote and local effects, arguing that the increase in cross-equatorial flow due to the remote effects of the strengthened Asian winter monsoon was insufficient to offset the suppression of the Australian summer monsoon caused by the atmospheric-response to orbital forcing. In their study, local ocean feedback resulting in the creation of an anomalously strong low pressure center in the tropical Indian Ocean was required to produce increased rainfall over northern Australia. Our analyses (Fig. 9) show that the location and enhancement of the low pressure cell in the Indian Ocean varies considerably from model to model, and FOAM is the only model that produces such a strong low pressure cell immediately offshore from the Australian continent. Hence, it is not surprising that it produces such a strong precipitation response in comparison with other models.

4.6 South America

Much of subtropical South America is characterised by monsoonal precipitation, associated with the development of upper-level anticyclonic circulation (Bolivian High) and low-level cyclonic circulation (Lenters and Cook 1995; Zhou and Lau 1998; Gan et al. 2004; Garreaud et al. 2008). In austral summer, maximum heating occurs in the subtropics (Fig. 2d) and a thermal low (Chaco Low) develops over the Paraguayan-Argentinean Gran Chaco and the Pampean sierras (Fig. 2e). Cross-equatorial flow, originating from the tropical Atlantic, is guided by the ridge of the Andes and circulates cyclonically around the Gran Chaco low (Fig. 2e). This flow attains a northwesterly direction in the Amazon region, where it converges with easterlies emanating from the South Atlantic high and results in a precipitation maximum over Amazonia. Over subtropical South America, the low-level flow is north-northwesterly, along the eastern foothills of the tropical and subtropical Andes. This flow convergences with northerlies along the western edge of the South Atlantic subtropical high and midlatitude southwesterlies to form a large-scale convergence zone (South Atlantic convergence zone), which results in a precipitation maximum extending southeastward from the southern Amazon towards southeast Brazil and the neighbouring Atlantic Ocean (Fig. 2f). A third precipitation maximum occurs over the central Andes, associated with orographic uplift along the eastern slopes and meridional wind convergence at higher elevations (Lenters and Cook 1995). These three precipitation maxima (>6 mm/day) are well reproduced in the PMIP control simulations (see e.g. Fig. 2f). The positions and magnitudes of some of the precipitation maxima (especially those in the east: Amazon and the South Atlantic Convergence Zone) are moderately affected by the longitudal structure of SSTs (Moura and Shukla 1981; Mechoso et al. 1990; Diaz et al. 1998), although this is not the dominant influence on the structure of the modern precipitation field.

The direct insolation effect decreases South America monsoon precipitation by ca −0.70 mm/day compared to

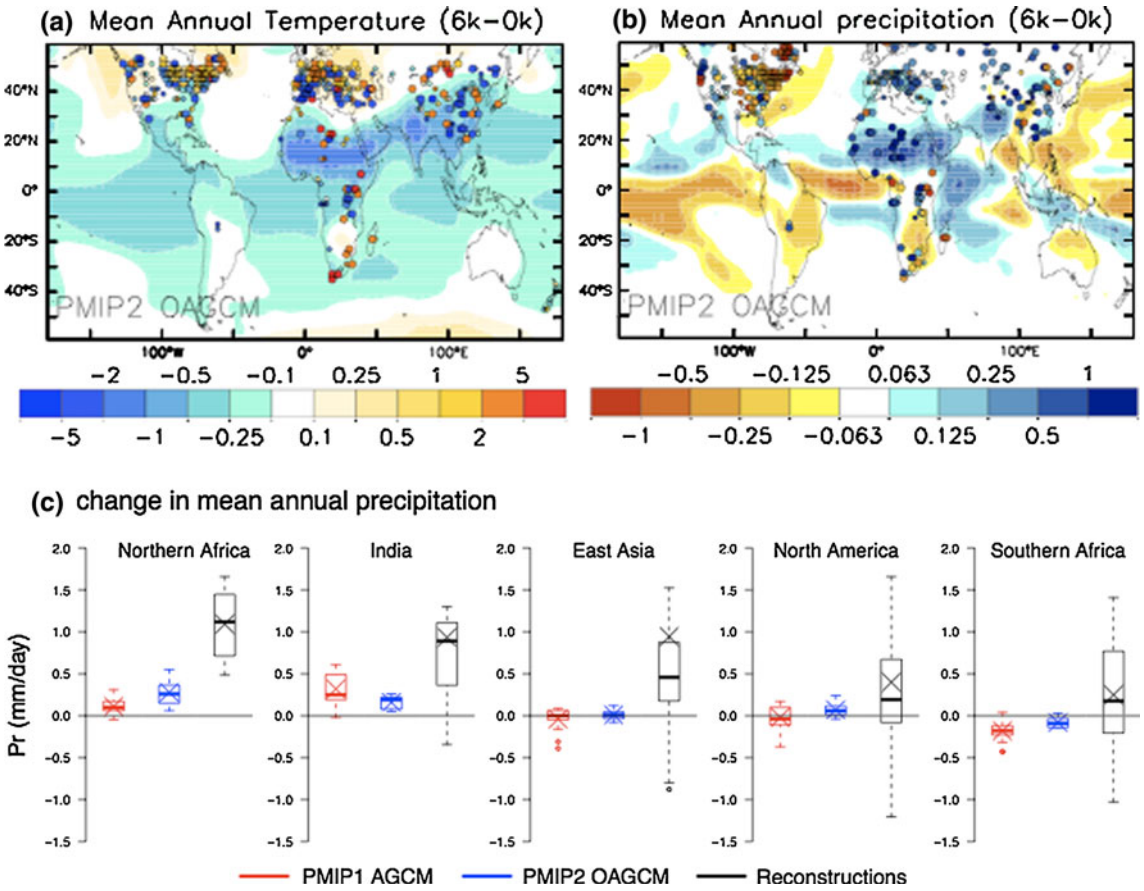

Fig. 10 Simulated changes in climate and pollen-based reconstructions. **a** Mean annual temperature (*MAT*); **b** mean annual precipitation (*MAP*) from 11-member PMIP2-OAGCM ensemble; **c** box-and-whisker plot of simulated and observed regional-mean MAP. In **a** and **b**, the *color shades* are the 11-member PMIP2-OAGCM ensemble mean; *dots* are from reconstructions, where *large symbols* are used to indicate grid points with significant anomalies while *small symbols* are used to indicate anomalies that are not significant. In **c** the columns (from *left* to *right*) are simulated change in MAP from the PMIP1 AGCM (*red*), PMIP2 OAGCM (*blue*) and reconstructions (*black*). The *bottom* and *top* of the *box* are the 25th and 75th percentile, respectively, and the band near the *middle* of the *box* is the median of regional mean of MAP across the17 PMIP1 AGCM and 11 PMIP2 OAGCM experiments, respectively. The ensemble mean change in MAP from the PMIP1 OAGCM simulations is shown by *red crosses*, while the ensemble mean change in MAP from the PMIP2 OAGCM simulations is shown by *blue crosses*. For the reconstructions, the band is the median MAP across all the grids with reconstructions. The *low* and *upper ends* of whiskers represent the minimum and maximum grid value, respectively. The weighted regional mean change in MAP is shown by *black crosses*. The regional domain for each monsoon region is defined in Table 3

present (Fig. 5g, left) and by −0.69 mm/day in the 5-member ensemble, whereas the decrease for the PMIP2 OAGCM ensemble (compared to present) is only −0.49 mm/day (Fig. 5g, right) and only −0.52 mm/day in the 5-member ensemble. Thus, ocean feedback appears to minimize the orbitally-induced reduction in precipitation. Although there is considerable inter-model variation in the decrease in precipitation, both in the PMIP1 AGCM (from −1.20 mm/day in BMRC to −0.23 mm/day in GISS) and PMIP2 OAGCM (from −1.11 mm/day in HADCM3 to −0.13 mm/day in ECBILT), the overall direction of the change in response to direct orbital forcing and ocean feedback is consistent and significant at the 90% level (Table 6).

The reduction in insolation in austral summer compared to present day (Fig. 1a) results in lower temperatures (ca −0.41°C) over South America (Fig. 3d; Table 4); the maximum decrease of >0.7°C occurs over the Gran Chaco region. As a result of the decrease in temperature, the thermal low over South America is weakened (ca −0.5 to −1.0 hPa, Fig. 3e) and land-sea contrast is reduced, resulting in reduced surface inflow and decreased monsoon precipitation (ca −1.0 mm/day, Fig. 3f). Land temperatures are further reduced (to ca −0.53°C) in the PMIP2 OAGCM simulations (Table 4), but the reduction over the Gran Chaco region is less pronounced (<−0.5°C; Fig. 4e). Thus, the weakening of the thermal low is not as marked in the PMIP2 OAGCM simulations and the reduction in monsoon precipitation is correspondingly less.

Our results are not consistent with previous analyses of the South American monsoon by Liu et al. (2004).

Although they also found that monsoon precipitation over South America was reduced as a result of the atmospheric response to mid-Holocene changes in insolation, ocean feedback produced a small but significant further reduction in the monsoon in their simulations. In contrast, our analyses (see also Rojas and Moreno 2011) indicate that the ocean feedback moderates the effect of direct orbital forcing such that the overall suppression of the South American monsoon is less than might otherwise be expected. A version of FOAM is included in the PMIP2 OAGCM ensemble, but we cannot check whether this version of the model produces similar results to those shown by Liu et al. (2004) because there is no comparable PMIP1 AGCM simulation in the PMIP ensemble. We speculate that the anomalous results of the earlier FOAM simulation may be related to deficiencies in the simulated cycle of precipitation: all of the other PMIP2 OAGCMs produce a modern (control) seasonal cycle that mimics observations with a relatively flat maximum from December through March. FOAM, on the other hand, has two precipitation maxima, in December and March/April; with precipitation levels significantly higher (>2 mm/day) than observed. In both the original Liu et al. (2004) and in the simulation from the PMIP ensemble, FOAM produces a large decrease in precipitation (compared with control) in every month throughout austral summer half-year.

5 Model-data comparison

The Bartlein et al. (2011) set does not contain information for the South America and northern Australia monsoon regions. Our focus here, then, is on evaluation of the other monsoon regions. Bartlein et al. (2011, their Fig. 6) present mapped reconstructions for multiple climate variables. Although drawing on all of these variables, we only present the MAT reconstructions visually (Fig. 10).

5.1 Northern Africa

The reconstructions for northern Africa show warmer summers than today, whether this is measured by the integrated temperature sum during the growing season (GDD5) or by the mean temperature of the warmest month (MTWA). The reconstructed MTWA is 2.44°C warmer than today. Most sites in the region register winters cooler than present, as measured by the mean temperature of the coldest month (MTCO); however, this cooling (−1.88°C) is not enough to offset the summer warming which translates into ca 1°C higher than present mean annual temperature (Fig. 10a). The simulations underestimate the summer warming: the PMIP1 AGCM ensemble shows an increase in MTWA of 0.80°C while the increase in the PMIP2 OAGCM ensemble is only 0.25°C. The simulated change in MTCO is more comparable to the observations; MTCO is decreased by −1.35°C in PMIP1 AGCM ensemble and by −1.29°C in the PMIP2 OAGCM ensemble. The simulations show the enhanced seasonal differences in temperature documented by the reconstructions, but as a result of the comparatively small summer warming, simulated MAT is lower than today in contrast to the reconstructions which show MAT higher than present.

The reconstructions show a significant increase in mean annual precipitation (1.15 mm/day), a signal which is assumed to be dominated by the increase in summer monsoon precipitation (Fig. 10b). Both sets of simulations show increased mean annual precipitation, with a mean increase of 0.11 mm/day for the PMIP1 AGCM and 0.28 mm/day for the PMIP2 OAGCM simulations (Table 5). The simulated increase is considerably less than the reconstructed change (Fig. 10c, d), although the underestimation of MAP is smaller in the case of the PMIP2 OAGCM simulations than the PMIP1 AGCM simulations. Estimating the change in simulated precipitation based only on those model grid cells for which there are reconstructions makes no differences to the magnitude of the simulated change or the discrepancy between the simulations and the reconstructions, so the mismatch is not likely to be a consequence of inadequate sampling. The underestimation of the change in precipitation over the northern Africa monsoon region in atmosphere-only simulations compared to observations was first noted by Joussaume et al. (1999), and the reduction in the discrepancy as a result of ocean feedback by Harrison (2000) (see also Braconnot et al. 2007).

5.2 India

There is very little data from the Indian monsoon region, and most of the reconstructions come from the northern part of the domain (beyond the northern front of the modern monsoon). There are no reconstructions of seasonal temperature anomalies, but reconstructed MAT is −0.23°C colder than present. Simulated MAT is also colder, but the anomalies are larger than shown by the reconstructions: −0.90°C in the case of the PMIP1 AGCM simulations and −0.76°C for the PMIP2 OAGCM simulations. The reconstructions show a increase in MAP of 0.93 mm/day (ca 95% more than present). The simulated increase in MAP is 0.32 mm/day in the PMIP1 AGCM simulations, but only 0.16 mm/day in the PMIP2 OAGCM simulations (Table 5). The discrepancy between the simulated and observed change in MAP is slightly larger when only those grid cells that contain observations are considered. The fact that there is closer agreement between the PMIP1 AGCM results and the reconstructions suggests that

the more muted increase in the monsoon produced by ocean feedback in the PMIP2 OAGCM simulations is unrealistic.

5.3 East Asia

There are no reconstructions of summer or winter temperature from the core East Asian monsoon region, although there are reconstructions from four grid cells in the northernmost part of the domain. The limited observations show warming in summer and cooling in winter, as do the simulations. However, the region is well covered by reconstructions of MAT. Reconstructed MAT shows conditions cooler than present by −1.36°C, consistent with, though larger than, the change shown in the PMIP1 AGCM (−0.48°C) and the PMIP2 OAGCM (ca −0.45°C) simulations. The reconstructions show a regionally-coherent increase in MAP across the region, with a 20% increase in precipitation in the southeast rising to a 100% increase compared to present in northwest China. The regional increase in MAP is ca 0.95 mm/day. The simulated changes in MAP are spatially complex: although precipitation is increased in northern and southern China, the central part of the region is generally characterised by a decrease in precipitation. As a result, there is no significant change in MAP compared to present in either set of simulations.

5.4 North America

The reconstructions for the North American monsoon region show cooling in summer, whether this is measured by GDD5 or by MTWA, and a year-round cooling of ca −1.1°C. The reconstructions show an increase in MAP of ca 0.42 mm/day, which is regionally coherent even though many of the individual site reconstructions are not significant. The simulations do not show summer cooling. However, simulated MAT is cooler than today, by −0.48°C in the PMIP1 AGCM and by −0.58°C in the PMIP2 OAGCM simulations, consistent with the reconstructed changes. The PMIP1 AGCM simulations do not show an increase in MAP, and although the PMIP2 OAGCM simulations show an increase of 0.07 mm/day the intermodal variance is larger than this. Furthermore, the simulated increase in precipitation is considerably less than the reconstructed increase (Fig. 10c), although the PMIP2 OAGCM simulations are more consistent with the reconstructions than the PMIP1 AGCM simulations.

5.5 Southern Africa

The reconstructions for the southern Africa monsoon region show warmer summers and warmer-than-present MAT, although some sites in the northeastern part of this domain (i.e. in the east African rift) show colder conditions both in summer and year-round. This is not consistent with the simulations, which show cooling in summer, and either cooling (PMIP2 OAGCM) or a slight warming (PMIP1 AGCM) for MAT. The reconstructions show an increase in MAP of ca 0.25 mm/day, which is not consistent with the simulations which show a decrease in MAP of −0.18 mm/day (PMIP1 AGCM) and −0.08 mm/day (PMIP2 OAGCM) respectively.

6 Summary and discussion

In this study, we have examined the response of the monsoons to 6 ka orbital forcing in the northern and southern hemisphere using 17 PMIP1 AGCMs and 11 coupled PMIP2 OAGCMs. This approach cannot provide an absolute discrimination of ocean feedback (or possible synergistic effects) that would be possible with a single model. Our analytical approach is constrained by changes in model configuration between the two phase of PMIP, and the fact that very few modelling groups were able to run atmosphere-only simulations during PMIP2. Nevertheless, the analyses yield insights into the role of ocean feedback in monsoon climates and raise a number of issues about the robustness of this feedback mechanism in specific regions that we hope will be addressed during the current phase of PMIP (PMIP3: Braconnot et al. 2011) analyses.

The atmospheric response to increased insolation in the northern subtropics strengthens the northern-hemisphere summer monsoons and leads to increased monsoonal precipitation in western North America, northern Africa and East Asia; ocean feedbacks amplify this response and lead to further increase in monsoon precipitation in these three regions. The atmospheric response to reduced insolation in the southern subtropics weakens the southern-hemisphere summer monsoons and leads to decreased monsoonal precipitation in South America, southern Africa and northern Australia; ocean feedbacks weaken this response so that the decrease in rainfall is smaller than might otherwise be expected. The role of the ocean in monsoonal circulation in equatorial regions is more complex. There is no discernable impact of orbital forcing in the monsoon region of North America in the atmosphere-only simulations but a strong increase in precipitation in the ocean–atmosphere simulations. In contrast, there is a strong atmospheric response to orbital forcing over northern India but ocean feedback reduces the strength of the change in the monsoon although it still remains stronger than today.

The response of individual monsoon systems to mid-Holocene orbital forcing and ocean feedbacks has been studied by individual modelling groups (e.g. Kutzbach and

Liu 1997; Hewitt and Mitchell 1998; Braconnot et al. 2000, 2004; Voss and Mikolajewicz 2001; Liu et al. 2004; Ohgaito and Abe-Ouchi 2007, Marzin and Braconnot 2009). Our analysis demonstrates the importance of using multi-model ensembles to determine the robustness both of the patterns of change and of the underlying mechanisms (see also Wang et al. 2010). We have shown, for example, that the mid-Holocene enhancement of the Australian monsoon shown in the FOAM simulations (Liu et al. 2004; Marshall and Lynch 2006) is not characteristic of other models. The PMIP ensemble demonstrates that, as with the other southern hemisphere monsoon systems, ocean feedbacks mitigate the insolation-induced reduction of the Australian monsoon but not sufficiently to produce increased precipitation over the continent. The difference in response can be traced back to inter-model differences in the location of the low pressure cell in the tropical Indian Ocean: while all of the coupled models produce an enhancement of the low pressure cell, FOAM is the only model that locates this cell immediately offshore from the Australian continent. The response of the North American monsoon to ocean feedback provides another example of the how the behaviour of a single model may be different to the general pattern of response. Most of the OAGCMs produce an enhancement of monsoon precipitation. The IPSL model shows a reduction in the strength of the North American monsoon in response to mid-Holocene orbital forcing and ocean feedback, most probably because of the model's pronounced cold bias over the tropical Pacific Ocean. Anomalous behaviour is not, of itself, a demonstration that the simulated response (and underlying mechanisms) is wrong; only detailed, quantitative comparisons with palaeoenvironmental observations can determine whether models produce the correct response to changes in forcing. However, the identification of anomalous behaviour through analysis of multi-model ensembles helps to identify the degree of uncertainty inherent in model-based explanations of past climate changes.

Our study also demonstrates that the analysis of individual simulations may be insufficient to identify the range of the mechanisms implicated in monsoon changes in specific regions. Previous studies of the North American monsoon (e.g. Harrison et al. 2003), for example, have emphasised the importance of the dipole structure in the eastern Pacific for the enhancement of monsoon precipitation. Our analyses suggest that the North American monsoon is also influenced by atmospheric conditions over the Atlantic, where the weakening of the subtropical high in conjunction with the strengthening of the monsoon trough leads to increased moisture convergence. As a second example, previous studies of the response of the mid-Holocene Indian monsoon to ocean feedback (e.g. Hewitt and Mitchell 1998; Braconnot et al. 2000; Liu et al. 2004) have emphasised that moisture flow into the subcontinent is strongly influenced by changes in strength of convection over the western tropical North Pacific. However, our analyses have shown that changes in SSTs in the Arabian Sea also have an important role to play. The orbitally-induced cooling of this region, which is the primary moisture source for the Indian monsoon, in spring and summer leads to delayed onset and an overall reduction in the strength of the monsoon.

In trying to understand differences between our analyses and previous studies, we have shown that conclusions can be influenced by decisions about the regions of interest as well as by the procedures used to derive regional climate averages. The different conclusions about the role of ocean feedback on the Indian monsoon reached by Hewitt and Mitchell (1998) and Liu et al. (2004), for example, can be directly related to the fact that the two studies used different definitions of the region affected by the monsoon: Hewitt and Mitchell (1998) included a larger part of Southeast Asia in the region used for calculating the change in monsoon precipitation than Liu et al. (2004). Since ocean feedback produces a reduction in monsoon precipitation over India and an increase in monsoon precipitation over Southeast Asia, this decision led to different conclusions in the two studies. Differences in the precise specification of which model cells contribute to area averages can also influence the results, as our analyses of the different magnitude of the change in the Australian monsoon simulated by FOAM in this study and values previously quoted by Liu et al. (2004) show. Tests of the sensitivity of our results to the definition of the monsoon domain indicate that, while there is very little impact on the results from e.g. north Africa or eastern Asia, there is an impact in regions where the domain includes oceanic grid cells because inter-model variance in precipitation is much larger over land than ocean.

Our comparison of simulated and reconstructed changes in temperature and precipitation, using the Bartlein et al. (2011) data set, suggests that coupled OAGCMs produce more realistic mid-Holocene climate changes, both with respect to MAT and MAP in the northern hemisphere monsoon regions. Nevertheless, the simulations considerably underestimate the increase in MAP in each of these regions. This underestimation has already been noted for northern Africa (Joussaume et al. 1999; Coe and Harrison 2002; Braconnot et al. 2007) but has escaped comment for other regions because of the reliance on qualitative climate reconstructions for data-model comparison (see e.g. Harrison et al. 2003; Wang et al. 2010). Lack of a network of quantitative reconstructions from South America and northern Australia precludes detailed data-model comparisons for these monsoon systems. In the case of southern Africa, the simulations show drier while the reconstructions

show wetter conditions. Although the discrepancy is smaller in the PMIP2 OAGCM simulations, nevertheless ocean feedback does not produce a reversal of the sign of precipitation change. The lack of agreement between the simulated and reconstructed climate of southern Africa suggests that our ability to simulate the Southern Hemisphere monsoons correctly is limited.

Our analyses emphasise the importance of ocean feedback in the response of the global monsoons to orbital forcing in the mid-Holocene, and demonstrate that the role of ocean feedback at a regional level is not always straight forward since the impact of ocean feedbacks varies both in sign and in magnitude from region to region. Other feedbacks, for example biophysical feedbacks related to vegetation changes (Kutzbach et al. 2001), may also be important and regionally complex. The use of multi-model ensembles, as promoted by PMIP, will therefore be important in order to derive a robust understanding of past climate changes. However, diagnosis of these simulations in order to identify correct response to initial forcings and feedbacks is reliant on the existence of networks of high-quality, well-dated palaeoclimatic reconstructions. There are obvious deficiencies in the spatial coverage of such reconstructions for many monsoon regions and particularly the southern hemisphere monsoon regions. Further efforts are required to remedy this situation in order to be able to evaluate model simulations comprehensively.

Acknowledgments We acknowledge the modeling groups participating in PMIP for providing their data for analysis, and the Laboratoire des Sciences du Climat et de l'Environnement (LSCE) for collecting and archiving the model data. We would like to thank Jean-Yves Peterschmitt for his help in extracting the model fields. The PMIP2/MOTIF Data Archive is supported by CEA, CNRS, the EU project MOTIF (EVK2-CT-2002-00153) and the Programme National d'Etude de la Dynamique du Climat (PNEDC). The analyses were performed using the version 12/10/2006 of the database. More information on the simulations is available on http://www-lsce.cea.fr/pmip/ and http://www-lsce.cea.fr/motif/. This paper is a contribution to the ORMEN project and to PMIP. We thank Patrick Bartlein for a very helpful review of this paper. We are also grateful to Pascale Braconnot for fruitful discussions.

References

Adams DK, Comrie AC (1997) The North American monsoon. Bull Am Meteorol Soc 78:2197–2213

An ZS (2000) The history and variability of the East Asian paleomonsoon climate. Q Sci Rev 19:171–187

An ZS, Porter SC, Kutzbach JE, Wu XH, Wang SM, Liu XD, Li XQ, Zhou WJ (2000) Asynchronous Holocene optimum of the East Asian monsoon. Q Sci Rev 19:743–762

Bartlein PJ, Harrison SP, Brewer S, Connor S, Davis BAS, Gajewski K, Guiot J, Harrison-Prentice TI, Henderson A, Peyron O, Prentice IC, Scholze M, Seppä H, Shuman B, Sugita S, Thompson RS, Viau AE, Williams J, Wu H (2011) Pollen-based continental climate reconstructions at 6 and 21 ka a global synthesis. Clim Dyn, doi:10.1007/s00382-010-0904-1

Beaufort L, van der Kaars S, Bassinot FC, Moron V (2010) Past dynamics of the Australian monsoon: precession, phase and links to the global monsoon concept. Clim Past 6:695–706

Behling H (1995) A high-resolution Holocene pollen record from Lago Do Pires, SE Brazil—vegetation, climate and fire history. J Paleolimnol 14:253–268

Berger AL (1978) Long-term variations of daily insolation and Quaternary climatic changes. J Atmos Sci 35:2362–2367

Braconnot P, Joussaume S, Marti O, de Noblet N (1999) Synergistic feedbacks from ocean and vegetation on the African monsoon response to mid-Holocene insolation. Geophys Res Lett 26:2481–2484

Braconnot P, Marti O, Joussaume S, Leclainche Y (2000) Ocean feedback in response to 6 kyr BP insolation. J Clim 13:1537–1553

Braconnot P, Loutre MF, Dong B, Joussaume S, Valdes P (2002) How the simulated change in monsoon at 6 ka BP is related to the simulation of the modern climate: results from the Paleoclimate Modeling Intercomparison Project. Clim Dyn 19:107–121

Braconnot P, Harrison SP, Joussaume S, Hewitt C, Kitoh A, Kutzbach J, Liu Z, Otto-Bliesner B, Syktus J, Weber SL (2004) Evaluation of PMIP coupled ocean-atmosphere simulations of the mid-Holocene. In: Battarbee RW, Gasse F, Stickley CE (eds) Past climate variability through Europe and Africa. Springer, Dordrecht, pp 515–533

Braconnot P, Otto-Bliesner B, Harrison S, Joussaume S, Peterchmitt J, Abe-Ouchi A, Crucifix M, Driesschaert E, Fichefet T, Hewitt CD, Kageyama M, Kitoh A, Laîné A, Loutre MF, Marti O, Merkel U, Ramstein G, Valdes P, Weber SL, Yu UQ, Zhao Y (2007) Results of PMIP2 coupled simulations of the Mid-Holocene and Last Glacial Maximum: Part 2: feedbacks with emphasis on the location of the ITCZ and mid- and high latitudes heat budget. Clim Past 3:279–296

Braconnot P, Harrison SP, Otto-Bliesner B, Abe-Ouchi A, Jungclaus J, Peterschmitt J-Y (2011) The paleoclimate modeling intercomparison project contribution to CMIP5. Clivar Newlett 56:15–19

Bush ABG (2002) A comparison of simulated monsoon circulations and snow accumulation in Asia during the mid-Holocene and at the Last Glacial Maximum. Global Planet Change 32:331–347

Carré M, Azzoug M, Bentaleb I, Chase BM, Fontugne M, Jackson D, Ledru M, Maldonado A, Sachs JP, Schauer AJ. Mid-Holocene mean climate in the south eastern Pacific and its influence on South America. Q Int (in press)

Chang CP (2004) East Asian Monsoon. World scientific series on meteorology of East Asia, vol 2. World Scientific, Singapore

Christensen JH, Hewitson B, Busuioc A, Chen A, Gao X, Held I, Jones R, Kolli RK, Kwon WT, Laprise R, Magaña Rueda V, Mearns L, Menéndez CG, Räisänen J, Rinke A, Sarr A, Whetton P (2007) Regional climate projections. In: Solomon S, Qin D, Manning M, Chen Z, Marquis M, Averyt KB, Tignor M, Miller HL (eds) Climate change 2007: the physical science basis. Contribution of working group I to the fourth assessment report of the intergovernmental panel on climate change. Cambridge University Press, Cambridge

Clark CO, Cole JE, Webster PJ (2000) Indian Ocean SST and Indian summer rainfall: predictive relationships and their decadal variability. J Clim 13:4452–4452

Coe MT, Harrison SP (2002) The water balance of northern Africa during the mid-Holocene: an evaluation of the 6 ka BP PMIP simulations. Clim Dyn 19:155–166

Colman RA, McAvaney BJ (1995) Sensitivity of the climate response of an atmospheric general circulation model to changes in convective parameterization and horizontal resolution. J Geophys Res 100:3155–3172

Cruz FW, Burns SJ, Karmann I, Sharp WD, Vuille M, Cardoso AO, Ferrari JA, Silva Dias PL, Viana O (2005) Insolation-driven changes in atmospheric circulation over the past 116,000 years in subtropical Brazil. Nature 434:63–66

Davidson NE, McBride JL, McAvaney BJ (1983) The onset of the Australian Monsoon during Winter Monex—synoptic aspects. Mon Weather Rev 111:496–516

Deque M, Dreveton C, Braun A, Cariolle D (1994) The ARPEGE/IFS atmosphere model: a contribution to the French community climate modelling. Clim Dyn 10:249–266

Diaz AF, Studzinski CD, Mechoso CR (1998) Relationships between precipitation anomalies in Uruguay and southern Brazil and sea surface temperature in the Pacific and Atlantic oceans. J Clim 11:251–271

Ding YH (1994) Monsoons over China. Kluwer, Dordrecht, p 419

Ding YH, Liu YJ (2001) Onset and the evolution of the summer monsoon over the South China Sea during SCSMEX field experiment in 1998. J Meteorol Soc Jpn 79:255–276

Doherty R, Kutzbach J, Foley J, Pollard D (2000) Fully coupled climate/dynamical vegetation model simulations over Northern Africa during the mid-Holocene. Clim Dyn 16:561–573

Douglas MW, Maddox RA, Howard K, Reyes S (1993) The Mexican monsoon. J Clim 6:1665–1677

Gan MA, Kousky VE, Ropelewski C (2004) The South Ameriça monsoon circulation and its relationship to rainfall over West-Central Brazil. J Clim 17:47–66

Garreaud R, Vuille M, Compagnucci R, Marengo J (2008) Present-day South American climate. Palaeo Palaeo Palaeo 281:180–195

Gordon HB, O'Farrell SP (1997) Transient climate change in the CSIRO coupled model with dynamic sea ice. Mon Weather Rev 125:875–907

Gordon CT, Stern WF (1982) A description of the GFDL global spectral model. Mon Weather Rev 110:625–644

Gordon C, Cooper C, Senior CA, Banks H, Gregory JM, Johns TC, Mitchell JFB, Wood RA (2000) The Simulation of SST, sea-ice extents and ocean heat transports in a version of the Hadley Centre Model without flux adjustments. Clim Dyn 16:147–168

Haak H, Jungclaus J, Mikolajewicz U, Latif M (2003) Formation and propagation of great salinity anomalies. Geophys Res Lett 30:1473. doi:10.1029/2003GL017065

Hall NM, Valdes PJ (1997) A GCM simulation of the climate 6000 years ago. J Clim 10:3–17

Hansen J, Mki S, Ruedy R (1997) Radiative forcing and climate response. J Geophys Res 102:6831–6864

Harrison SP, Braconnot P, Joussaume S, Hewitt C, Stouffer RJ (2002) Comparison of palaeoclimate simulations enhance confidence in models. EOS 83:447

Harrison SP, Kutzbach JE, Liu Z, Bartlein PJ, Otto-Bliesner B, Muhs D, Prentice IC, Thompson RS (2003) Mid-Holocene climates of the Americas: a dynamical response to changed seasonality. Clim Dyn 20:663–688

Hastenrath S (1994) Climate dynamics of the tropics. Kluwer, Dordrecht, p 488

Haug GH, Hughen KA, Sigman DM, Peterson LC, Röhl U (2001) Southward migration of the Intertropical Convergence Zone through the Holocene. Science 293:1304–1308

Hewitt CD, Mitchell JFB (1996) GCM simulations of the climate of 6 kyr BP: mean changes and interdecadal variability. J Clim 9:3505–3529

Hewitt CD, Mitchell JFB (1998) A fully coupled GCM simulation of the climate of the mid-Holocene. Geophys Res Lett 25:361–364

Higgins RW, Shi W (2000) Dominant factors responsible for interannual variability of the summer monsoon in the south-western United States. J Clim 13:759–776

Higgins RW, Yao Y, Wang XL (1997) Influence of the North American monsoon system on the US summer precipitation regime. J Clim 10:2600–2622

Huang CC, Pang JL, Zhao JP (2000) Chinese loess and the evolution of the East Asian monsoon. Prog Phys Geogr 24:75–96

Jacob R, Schafer C, Foster I, Tobis M, Andersen J (2001) Computational design and performance of the fast ocean atmosphere model: version 1. In: The 2001 International Conference on Computational Science, pp 175–184

Johnson BJ, Miller GH, Fogel ML, Magee JW, Gagan MK, Chivas AR (1999) 65,000 years of vegetation change in central Australia and the Australian summer monsoon. Science 284:1150–1152

Joussaume S, Taylor KE (2000) Paleoclimate modeling intercomparison project (PMIP). In: Proceedings of the third PMIP workshop WCRP-111, p 271

Joussaume S, Taylor KE, Braconnot P, Mitchell JFB, Kutzbach JE, Harrison SP, Prentice IC, Broccoli AJ, Abe-Ouchi A, Bartlein PJ, Bonfils C, Dong B, Guiot J, Herterich K, Hewitt CD, Jolly D, Kim JW, Kislov A, Kitoh A, Loutre MF, Masson V, McAvaney B, McFarlane N, de Noblet N, Peltier WR, Peterschmitt JY, Pollard D, Rind D, Royer JF, Schlesinger ME, Syktus J, Thompson S, Valdes P, Vettoretti G, Webb RS, Wyputta U (1999) Monsoon changes for 6000 years ago: results of 18 simulations from the paleoclimate modeling intercomparison project (PMIP). Geophys Res Lett 26:859–862

K-1-Model-Developers (2004) K-1 coupled GCM (Miroc Description)1, Report no. 1, Center for Climate System Research, University of Tokyo, Tokyo

Kiehl JT, Hack JJ, Bonan GB, Boville BA, Briegleb BP, Williamson DL, Rasch PJ (1996) Description of the NCAR community climate model (CCM3), NCAR Tech. Note NCAR/TN–420 + STR, National Center for Atmospheric Research. Boulder, Colorado

Kitoh A, Noda A, Nikaidou Y, Ose T, Tokioka T (1995) AMIP simulations of the MRI GCM. Pap Met Geophys 45:121–148

Kohfeld KE, Harrison SP (2001) DIRTMAP: the geological record of dust. Earth-Sci Rev 54:81–114

Krishnamurti TN, Bhalme HN (1976) Oscillations of a monsoon system. 1. Observational aspects. J Atmos Sci 33:1937–1954

Kullgren K, Kim K-Y (2006) Physical mechanisms of the Australian summer monsoon: 1. Seasonal Cycle J Geophys Res 111:D20104. doi:10.1029/2005JD006807

Kutzbach JE, Guetter PJ (1986) The influence of changing orbital parameters and surface boundary-bonditions on climate simulations for the past 18000 years. J Atmos Sci 43:1726–1759

Kutzbach JE, Liu Z (1997) Response of the African monsoon to orbital forcing and ocean feedbacks in the middle Holocene. Science 278:440–443

Kutzbach JE, Otto-Bliesner BL (1982) The sensitivity of the African-Asian monsoonal climate to orbital parameter changes for 9000 years BP in a low-resolution general-circulation model. J Atmos Sci 39:1177–1188

Kutzbach J, Bonan G, Foley J, Harrison SP (1996) Vegetation and soil feedbacks on the response of the African monsoon to orbital forcing in the early to middle Holocene. Nature 384:623–626

Kutzbach JE, Harrison SP, Coe MT (2001) Land-ocean-atmosphere interactions and monsoon climate change: a paleo-perspective. In: Schulze E-D, Heimann M, Harrison SP, Holland E, Lloyd J, Prentice IC, Schimel D (eds) Global biogeochemical cycles in the climate system. Academic Press, London, pp 73–86

Lau KM, Kim KM, Yang S (2000) Dynamical and boundary forcing characteristics of regional components of the Asian summer monsoon. J Clim 13:2461–2482

Lenters JD, Cook KH (1995) Simulation and diagnosis of the regional summertime precipitation climatology of South America. J Clim 8:2988–3005

Li SL, Lu J, Huang G, Hu KM (2008) Tropical Indian Ocean Basin warming and East Asian summer monsoon: a multiple AGCM study. J Clim 21(22):6080–6088

Lim YK, Kim KY, Lee HS (2002) Temporal and spatial evolution of the Asian summer monsoon in the seasonal cycle of synoptic fields. J Clim 15:3630–3644

Liu Z, Harrison SP, Kutzbach JE, Otto-Bliesner B (2004) Global monsoons in the mid-Holocene and oceanic feedback. Clim Dyn 22:157–182

Lorenz S, Grieger B, Helbig P, Herterich K (1996) Investigating the sensitivity of the atmospheric general circulation model ECHAM3 to paleoclimatic boundary conditions. Geol Rundsch 85:513–524

Marshall AG, Lynch AH (2006) Time slice analysis of the Australian summer monsoon during the late Quaternary using the Fast Ocean Atmosphere Model. J Quaternary Sci 21:789–801

Marsland SJ, Haak H, Jungclaus JH, Latif M, Roske F (2003) The Max-Planck-Institute global ocean/sea ice model with orthogonal curvilinear coordinates. Ocean Model 5:91–127

Marti O, Braconnot P, Bellier J, Benshila R, Bony S, Brockmann P, Cadule P, Caubel A, Denvil S, Dufresne JL, Fairhead L, Filiberti MA, Foujols M-A, Fichefet T, Friedlingstein P, Goosse H, Grandpeix JY, Hourdin F, Krinner G, Lévy C, Madec G, Musat I, de Noblet N, Polcher J, Talandier C (2005) The new IPSL climate system model: IPSL-Cm4, Note du Pôle de Modélisation, n 26, ISSN 1288-1619

Marzin C, Braconnot P (2009) The role of the ocean feedback on Asian and African monsoon variations at 6kyr and 9.5kyr BP. Comptes Rendus Geosci 341:643–655

Masson V, Joussaume S (1997) Energetics of the 6000 BP atmospheric circulation in boreal summer, from large scale to monsoon areas: a study with two versions of the LMD AGCM. J Clim 10:2888–2903

Mechoso CR, Lyons SW, Spahr JA (1990) The impact of sea-surface temperature anomalies on the rainfall over northeast Brazil. J Clim 3:812–826

Miller GH, McGee JW, Johnson ML, Fogel NA, Spooner NA, McCulloch MT, Aycliffe LK (1999) Pleistocene extinction of *genyornis newtoni*: human impact on Australian megafauna. Science 283:205–208

Monnin E, Steig EJ, Siegenthaler U, Kawamura K, Schwander J, Stauffer B, Stocker TF, Morse DL, Barnola JM, Bellier B, Raynaud D, Fischer H (2004) Evidence for substantial accumulation rate variability in Antarctica during the Holocene, through synchronization of CO_2 in the Taylor Dome, Dome C and DML ice cores. Earth Planet Sci Lett 224:45–54

Moura AD, Shukla J (1981) On the dynamics of droughts in northeast Brazil—observations, theory and numerical experiments with a general-circulation model. J Atmos Sci 38:2653–2675

Nicholls N, McBride JL, Ormerod RJ (1982) On predicting the onset of the Australian wet aeason at Darwin. Mon Wea Rev 110:14–17

Ninomiya K, Kobayashi C (1999) Precipitation and moisture balance of the Asian summer monsoon in 1991 Part II: Moisture transport and moisture balance. J Meteorol Soc Jpn 77:77–99

Numaguti A, Takahashi M, Nakajima T, Sumi A (1997) Description of CCSR/NIES atmospheric general circulation model. CGER's supercomputer monograph report, center for global environmental research. National Institute for Environmental Studies 3:1–48

Ohgaito R, Abe-Ouchi A (2007) The role of ocean thermodynamics and dynamics in Asian summer monsoon changes during the mid-Holocene. Clim Dyn 29:39–50

Ohgaito R, Abe-Ouchi A (2009) The effect of sea surface temperature bias in the PMIP2 AOGCMs on mid-Holocene Asian monsoon enhancement. Clim Dyn 33:975–983

Otto J, Raddatz T, Claussen M, Brovkin V, Gayler V (2009) Separation of atmosphere-ocean-vegetation feedbacks and synergies for mid-Holocene climate. Geophys Res Lett 36. doi: 10.1029/2009GL037482.

Otto-Bliesner BL (1999) El Nino, La Nina and Sahel precipitation during the middle Holocene. Geophys Res Lett 26:87–90

Otto-Bliesner BL, Brady EC, Clauzet G, Tomas R, Levis S, Kothavala Z (2006) Last Glacial maximum and Holocene climate in CCSM3. J Clim 19:2526–2544

Overpeck J, Anderson D, Trumbore S, Prell W (1996) The southwest Indian Monsoon over the last 18000 years. Clim Dyn 12:213–225

Petit-Maire N (1989) Interglacial environments in presently hyperarid Sahara: palaeoclimatic implications. In: Leinen M, Sarnthein M (eds) Paleoclimatology and paleometerology: modern and past patterns of global atmospheric transport. Kluwer, Norwell, pp 637–661

Pollard D, Bergengren JC, Stillwell-Soller LM, Felzer B, Thompson SL (1998) Climate simulations for 10,000 and 6,000 years BP using the GENESIS global climate model. Paleoclim Data Model 2:183–218

Poore R, Pavich M, Grissino-Mayer H (2005) Record of the North American southwest monsoon from Gulf of Mexico sediment cores. Geology 33:209–212

Prentice C, Jolly D, BIOME 6000 Participants (2000) Mid-Holocene and glacial-maximum vegetation geography of the northern continents and Africa. J Biogeogr 27:507–519

Ramage R (1971) Monsoon meterology. Academic Press, New York, p 296

Rao KG, Goswami BN (1988) Interannual variations of sea-surface temperature over the Arabian Sea and the Indian Monsoon—a new perspective. Mon Weather Rev 116:558–568

Roeckner E, Bauml G, Bonaventura L, Brokopf R, Esch M, Giorgetta M, Hagemann S, Kirchner I, Kornblueh L, Manzini E, Rhodin A, Schlese U, Schulzweida U, Tompkins A (2003) The atmospheric general circulation model Echam5, Part I: model description, internal report 349, 144 pp

Rojas M, Moreno PI (2011) Atmospheric circulation changes and neoglacial conditions in the Southern Hemisphere mid-latitudes: insights from PMIP2 simulations at 6 kyr. Clim Dyn 37:357–375

Sadhuram Y, Kumar MRR (1988) Does evaporation over the Arabian Sea play a crucial role in moisture transport across the west-coast of India during an active monsoon period. Mon Weather Rev 116:307–312

Schlesinger ME, Andronova NG, Entwistle B, Ghanem A, Ramankutty N, Wang W, Yang F (1997) Modeling and simulation of climate and climate change. In: Past and present variability of the solar-terrestrial system: measurement, data analysis and theoretical models. Proceedings of the international school of physics "Enrico Fermi", Varrena, Italy. IOS Press, Amsterdam, pp 389–429

Schmidt GA, Hoffmann G, Shindell DT, Hu Y (2005) Modelling atmospheric stable water isotopes and the potential for constraining cloud processes and stratosphere-troposphere water exchange. J Geophys Res 110:D21314. doi:10.1029/2005JD005790

Shi YF, Kong ZZ, Wang SM, Tang LY, Wang FB, Yao TD, Zhao XT, Zhang PY, Shi SH (1993) Mid-holocene climates and environments in China. Global Planet Change 7:219–233

Shukla J (1975) Effect of Arabian sea-surface temperature anomaly on Indian summer monsoon—Numerical experiment with GFDL model. J Atmos Sci 32:503–511

Staubwasser M, Weiss H (2006) Holocene climate and cultural evolution in late prehistoric-early historic West Asia. Quaternary Res 66:372–387

Street-Perrott FA, Perrott R (1993) Holocene vegetation, lake levels and climate of Africa. In: Wright HE, Kutzbach JE, Webb T, Ruddiman WF, Street-Perrott FA, Bartlein PJ (eds) Global climates since the Last Glacial maximum. The University of Minnesota Press, Minneapolis, pp 318–356

Tao S, Chen L (1987) A review of recent research on the East Asian summer monsoon in China. In: Chang CP, Krishnamurti TN (eds) Monsoon meteorology. Oxford University Press, Oxford, pp 60–92

Texier D, de Noblet N, Braconnot P (2000) Sensitivity of the African and Asian monsoons to mid-Holocene insolation and data-inferred surface changes. J Clim 13:164–181

Thompson RS, Anderson KH (2000) Biomes of western North America at 18,000, 6000 and 0 C-14 yr BP reconstructed from pollen and packrat midden data. J Biogeogr 27:555–584

Tokioka T, Yamazaki K, Yagai I, Kitoh A (1984) A description of the meteorological research institute atmospheric general circulation model (MRI GCM-I). MRI Tech. Report No. 13, Meteorological Research Institute, Ibaraki-ken, Japan, 249 pp

Trenberth KE, Stepaniak DP, Caron JM (2000) The global monsoon as seen through the divergent atmospheric circulation. J Clim 13:3969–3993

Vera C, Higgins W, Amador J, Ambrizzi T, Garreaud R, Gochis D, Gutzler D, Lettenmaier D, Marengo J, Mechoso CR, Nogues-Paegle J, Silva Dias PL, Zhang C (2006) Toward a unified view of the American monsoon systems. J Clim 19:4977–5000

Vettoretti G, Peltier WR, McFarlane NA (1998) Simulations of Mid-Holocene climate using an atmospheric general circulation model. J Clim 11:2607–2627

Voss R, Mikolajewicz U (2001) The climate of 6000 years BP in near-equilibrium simulations with a coupled AOGCM. Geophys Res Lett 28:2213–2216

Vries P, Weber SL (2005) The Atlantic freshwater budget as a diagnostic for the existence of a stable shut-down of the meridional overturning circulation. Geophys Res Lett 32:L09606. doi:10.1029/2004GL021450

Wang B, Wu RG, Lau KM (2001) Interannual variability of the Asian summer monsoon: contrasts between the Indian and the western North Pacific-east Asian monsoons. J Clim 14:4073–4090

Wang T, Wang HJ, Jiang DB (2010) Mid-Holocene East Asian summer climate as simulated by the PMIP2 models. Palaeogeogr Palaeoclimatol Palaeoecol 288:93–102

Webster PJ, Magana VO, Palmer TN, Shukla J, Tomas RA, Yanai M, Yasunari T (1998) Monsoons: processes, predictability and the prospects for prediction. J Geophys Res 103:14451–14510

Wohlfahrt J, Harrison SP, Braconnot P (2004) Synergistic feedbacks between ocean and vegetation on mid- and high-latitude climates during the mid-Holocene. Clim Dyn 22:223–238

Wyrwoll KH, Miller GH (2001) Initiation of the Australian summer monsoon 14,000 years ago. Quaternary Int 83–5:119–128

Xue F, Wang H, He J (2003) Interannual variability of Mascarene high and Australian high and their influences on summer rainfall over East Asia. Chin Sci Bull 48:492–497

Yang S, Lau KM (1998) Influences of sea surface temperature and ground wetness on Asian summer monsoon. J Clim 11:3230–3246

Yu G, Chen X, Ni J, Cheddadi R, Guiot J, Han H, Harrison SP, Huang C, Ke M, Kong Z, Li S, Li W, Liew P, Liu G, Liu J, Liu Q, Liu KB, Prentice IC, Qui W, Ren G, Song C, Sugita S, Sun X, Tang L, VanCampo E, Xia Y, Xu Q, Yan S, Yang X, Zhao J, Zheng Z (2000) Palaeovegetation of China: a pollen data-based synthesis for the mid-Holocene and last glacial maximum. J Biogeogr 27:635–664

Yu YQ, Yu RC, Zhang XH, Liu HL (2002) A flexible coupled ocean-atmosphere general circulation model. Adv Atmos Sci 19:169–190

Yu YQ, Zhang XH, Guo YF (2004) Global coupled ocean-atmosphere general circulation models in Lasg/Iap. Adv Atmos Sci 21:444–455

Yukimoto S, Noda A, Kitoh A, Hosaka M, Yoshimura H, Uchiyama T, Shibata K, Arakawa O, Kusunoki S (2006) Present-day climate and climate sensitivity in the meteorological research institute coupled GCM version 2.3 (Mri-Cgcm2.3). J Meteorol Soc Jpn 84:333–363

Zhao ZC, Ding YH, Li XD, Wang SH (1995) Evaluation of CGCM climate simulation *in* East Asia region. J Appl Meterol Sci 6:9–18 (in Chinese)

Zhao Y, Braconnot P, Marti O, Harrison SP, Hewitt C, Kitoh A, Liu Z, Mikolajewicz U, Otto-Bliesner B, Weber SL (2005) A multi-model analysis of the role of the ocean on the African and Indian monsoon during the mid-Holocene. Clim Dyn 25:777–800

Zhou JY, Lau KM (1998) Does a monsoon climate exist over South America? J Clim 11:1020–1040